Article

Neuron

A Translational Repression Complex in Developing Mammalian Neural Stem Cells that Regulates Neuronal Specification

Highlights

- Radial precursors are transcriptionally primed to make diverse neuronal subtypes
- The 4E-T repressor forms a complex with Pum2 during neurogenesis
- Neuronal specification mRNAs are translationally repressed in radial precursors
- Disruption of the Pum2/4E-T complex causes misspecification of cortical neurons

Authors

Siraj K. Zahr, Guang Yang, Hilal Kazan, ..., Anastassia Voronova, David R. Kaplan, Freda D. Miller

Correspondence

fredam@sickkids.ca

In Brief

Zahr et al. show that cortical RPs are transcriptionally primed to generate diverse neuronal subtypes and that translational repression mechanisms determine which transcription factor mRNAs are translated to ensure appropriate temporal specification of daughter neurons.

Zahr et al., 2018, Neuron *97*, 520–537
February 7, 2018
https://doi.org/10.1016/j.neuron.2017.12.045

CellPress

CellPress

Neuron
Article

A Translational Repression Complex in Developing Mammalian Neural Stem Cells that Regulates Neuronal Specification

Siraj K. Zahr,[1,3] Guang Yang,[1,6] Hilal Kazan,[2] Michael J. Borrett,[1,3] Scott A. Yuzwa,[1] Anastassia Voronova,[1,7] David R. Kaplan,[1,3,4] and Freda D. Miller[1,3,4,5,8,*]

[1]Program in Neurosciences and Mental Health, Hospital for Sick Children, Toronto, ON M5G 1L7, Canada
[2]Department of Computer Engineering, Antalya Bilim University, Antalya, Turkey
[3]Institute of Medical Science
[4]Department of Molecular Genetics
[5]Department of Physiology
University of Toronto, Toronto, ON M5G 1A8, Canada
[6]Present address: HS2229, 3330 Hospital Drive N.W., University of Calgary, Calgary, AB T2N 1N4, Canada
[7]Present address: 8-32 Medical Sciences Building, University of Alberta, Edmonton, AB T6G 2H7, Canada
[8]Lead Contact
*Correspondence: fredam@sickkids.ca
https://doi.org/10.1016/j.neuron.2017.12.045

SUMMARY

The mechanisms instructing genesis of neuronal subtypes from mammalian neural precursors are not well understood. To address this issue, we have characterized the transcriptional landscape of radial glial precursors (RPs) in the embryonic murine cortex. We show that individual RPs express mRNA, but not protein, for transcriptional specifiers of both deep and superficial layer cortical neurons. Some of these mRNAs, including the superficial versus deep layer neuron transcriptional regulators *Brn1* and *Tle4*, are translationally repressed by their association with the RNA-binding protein Pumilio2 (Pum2) and the 4E-T protein. Disruption of these repressive complexes in RPs mid-neurogenesis by knocking down 4E-T or Pum2 causes aberrant co-expression of deep layer neuron specification proteins in newborn superficial layer neurons. Thus, cortical RPs are transcriptionally primed to generate diverse types of neurons, and a Pum2/4E-T complex represses translation of some of these neuronal identity mRNAs to ensure appropriate temporal specification of daughter neurons.

INTRODUCTION

Appropriate circuit assembly in the mammalian cerebral cortex requires the genesis of diverse excitatory neurons that differ in their morphology, connectivity, and function. These different neurons are all made by radial glial precursors (RPs) that generate neurons either directly or indirectly via transit-amplifying intermediate progenitor (IP) cells. The newborn neurons then migrate basally to form the nascent cortical layers, with the earliest-born neurons populating the deepest layers and later-born neurons progressively populating more superficial layers. Subsequent to this neurogenic period, which occurs from embryonic day 11 (E11) to E17 in the mouse, the same pool of RPs generates glial cells.

What determines this timed neuronal genesis, particularly in light of recent work showing that individual cortical RPs are multipotent and sequentially generate diverse cortical neurons (Guo et al., 2013; Gao et al., 2014; Eckler et al., 2015; Shen et al., 2006)? One attractive molecular explanation posits transcriptional induction of regulatory proteins that specify neuron subtypes as neurons are generated (Greig et al., 2013; Kwan et al., 2012). However, this model is complicated by the finding that RPs themselves express some neuronal specifiers at the mRNA, but not, protein level (Arlotta et al., 2005; Guo et al., 2013; Eckler et al., 2015), indicating that post-transcriptional regulation might also be important. In this regard, we recently identified a translational repression complex involving the 4E-T protein and showed that it determines the timing and extent of cortical neurogenesis by regulating the translation of proneurogenic bHLH proteins (Yang et al., 2014). These findings suggest a second, not mutually exclusive model in which cortical RPs are transcriptionally primed to make diverse neuronal subtypes and in which selective repression determines which specifiers are translated and, thus, which types of neurons are generated.

Here we have tested this model and provide evidence that, during embryonic neurogenesis, cortical RPs co-express mRNAs encoding specifiers for diverse cortical neuron subtypes and that a complex involving 4E-T and the RNA-binding protein Pumilio2 selectively represses translation of some of these mRNAs to ensure the appropriate specification of daughter neurons.

RESULTS

Single-Cell RNA Sequencing Demonstrates that Embryonic RPs Co-express mRNAs Encoding Specification Factors for Different Types of Cortical Neurons

To identify neuronal specification genes expressed by embryonic precursors, we analyzed recently published single-cell

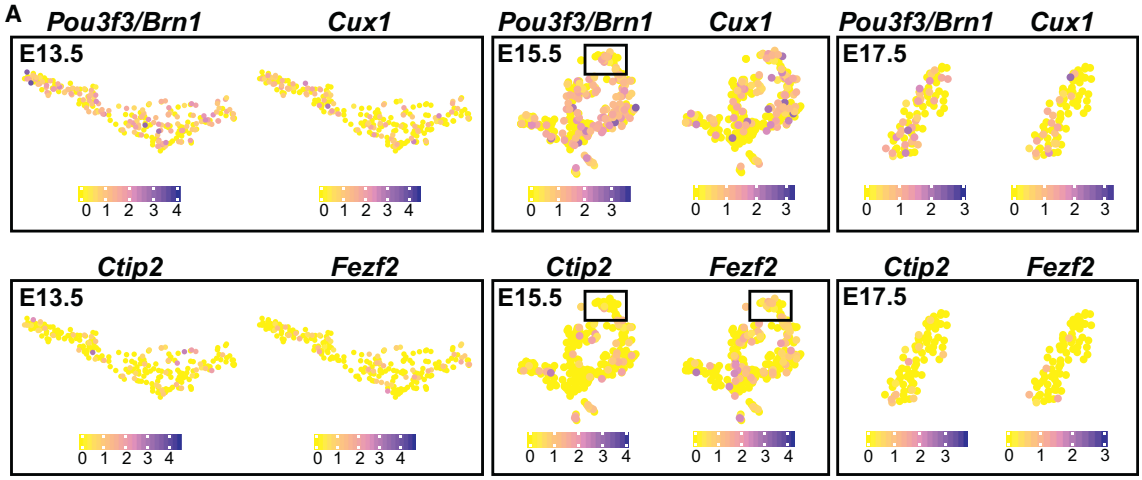

B

Gene	% E13.5 RPs	% E15.5 RPs	% E17.5 RPs
Brn1	55	51	38
Brn2	36	51	29
Lhx2	38	46	19
Cux1	34	33	25
Tle3	15	13	7
Tle1	24	27	17
Bhlhe22	1	3	4
Tle4	9	10	10
Ctip2	21	16	16
Fezf2	21	29	7
Otx1	13	14	7
Sox5	23	21	26
Lix1	12	13	7
Lmo4	20	19	31
Diap3	9	11	1
Foxp2	6	6	3
Tbr1	2	6	4

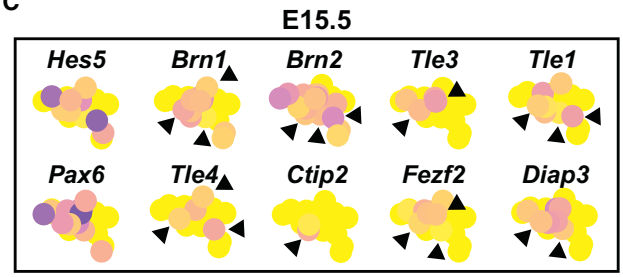

D

Age	% RPs expressing both DL and SL specifiers	% RPs expressing only SL specifiers	% RPs expressing only DL specifiers
E13.5	72	17	8
E15.5	73	21	4
E17.5	54	19	23

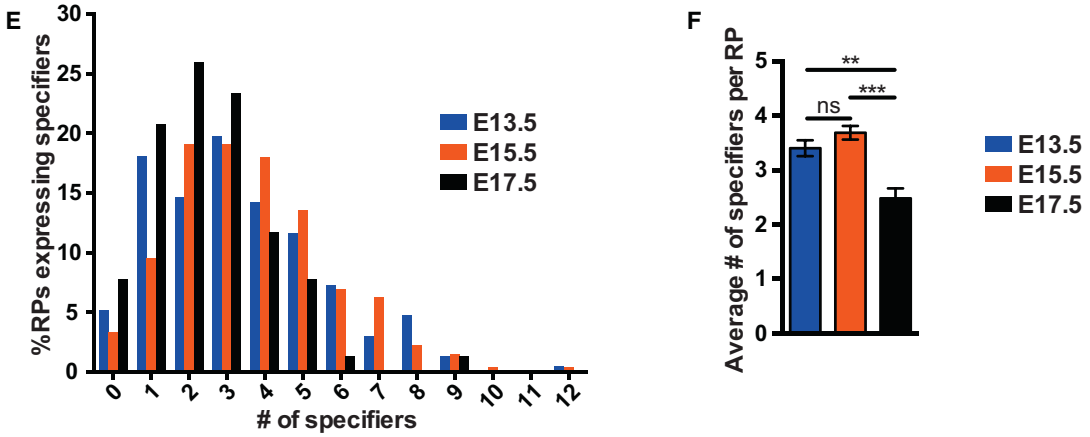

Figure 1. Individual Embryonic RPs Detectably Co-express Specification mRNAs, as Determined by scRNA-Seq

Analysis of scRNA-seq data from the E13.5, E15.5, and E17.5 RP clusters in Yuzwa et al. (2017) (GEO: GSE107122; Figure S1).

(A) t-SNE visualization of E13.5, E15.5, and E17.5 scRNA-seq data overlaid with expression of the superficial layer (SL) specifiers *Pou3f3/Brn1* and *Cux1* and the deep layer (DL) specifiers *Ctip2* and *Fezf2*. Cells are color-coded according to expression level, ranging from not detected (yellow) to the highest detected levels (blue), according to the adjacent color key. Boxed regions in the E15.5 images are shown at higher resolution in (C).

(B) Table showing the percentages of E13.5, E15.5, and E17.5 RPs expressing superficial and deep layer neuron specifiers.

(legend continued on next page)

RNA sequencing (scRNA-seq) data from the murine cortex obtained at E13.5, when both deep and superficial layer neurons are generated; at E15.5, when only superficial layer neurons are made; and at E17.5, when neurogenesis is over (Yuzwa et al., 2017; GEO: GSE107122). This study used droplet sequencing (Drop-seq) to transcriptionally profile 2,000–5,000 total cortical cells at each age and to define RPs, IPs, and neurons (Figure S1A). We focused on the RP clusters in these datasets, which included 233, 273, and 77 cells at E13.5, E15.5, and E17.5, respectively (Figure S1A).

We first analyzed the E13.5 and E15.5 RP transcriptomes for expression of 26 genes encoding proteins that specify and/or are associated with cortical neurons in different layers (termed specification genes). These included 13 genes for superficial layer neurons (*Pou3f3/Brn1*, *Pou3f2/Brn2*, *Lhx2*, *Cux1*, *Tle3*, *Tle1*, *Mef2c*, *Bhlhe22/Bhlhb5*, *Cux2*, *Pou3f1/Oct6*, *Kitl*, *Unc5d*, and *Satb2*) and 13 for deep layer neurons (*Tle4*, *Fezf2*, *Ctip2*, *Otx1*, *Sox5*, *Lix1*, *Lmo4*, *Diap3*, *Lxn*, *Foxp2*, *Tbr1*, *Ldb2*, and *Pcp4*). All of these mRNAs were detectably expressed in E13.5 neurons (see Figure S1B for examples; Yuzwa et al., 2017). Six superficial layer (*Pou3f3/Brn1*, *Pou3f2/Brn2*, *Lhx2*, *Cux1*, *Tle3*, and *Tle1*) and nine deep layer neuron mRNAs (*Tle4*, *Fezf2*, *Ctip2*, *Otx1*, *Sox5*, *Lix1*, *Lmo4*, *Diap3*, and *FoxP2*) were detectably expressed in 6%–55% of E13.5 and E15.5 RPs (Figures 1A and 1B). Visualizations using t-distributed stochastic neighbor embedding (t-SNE) indicated that among the most widely detected were the superficial layer specifiers *Pou3f3/Brn1* (51%–55%) and *Cux1* (33%–34%), and the deep layer specifiers *Fezf2* (21%–29%) and *Ctip2* (16%–21%) (Figures 1A and 1B). The remaining 11 genes were detectably expressed in $\leq$5% of E13.5 RPs (*Bhlhe22* [1%], *Cux2* [0.5%], *Pou3f1/Oct6* [3%], *Kitl* [3%], *Unc5d* [2%], *Satb2* [3%], *Mef2c* [2%], *Lxn* [5%], *Ldb2* [2%], *Pcp4* [4%], and *Tbr1* [2%]) and were not further analyzed, except for *Bhlhe22* and *Tbr1*, which were included as examples of neuron-enriched specification genes (Figure S1B).

The t-SNE visualizations also showed that many RPs co-expressed deep and superficial layer neuron specification mRNAs (Figure 1C). We quantified this by determining the proportion of E13.5 and E15.5 RPs that co-expressed the 15 superficial versus deep layer genes expressed in more than 5% of the RPs plus *Bhlhe22* and *Tbr1* (that is, the genes shown in Figure 1B). At both ages, $\geq$95% of cells in the RP clusters expressed at least one specification mRNA, and 72%–73% co-expressed both superficial and deep layer mRNAs. A distribution analysis (Figure 1E) showed that >50% of RPs at E13.5 and E15.5 expressed 3 or more specification genes (see Figure 1C for examples) and that about 10% expressed 6–10. Thus, from E13.5 to E15.5, most RPs are transcriptionally primed to make diverse cortical neurons. A similar analysis at E17.5, when neurogenesis is over, showed that all of the specification genes were still detectably expressed in at least some RPs (Figures 1A and 1B) and that many RPs still co-expressed superficial and deep layer neuron specification genes (Figure 1D). However, individual E17.5 RPs did not express as many specification genes as at the earlier time points, and very few expressed 6 or more (Figures 1E and 1F).

Deep and Superficial Layer Neuron Specification mRNAs Are Co-expressed in RPs throughout Neurogenesis

We further characterized the co-expression of neuronal specification genes in RPs by performing single-molecule fluorescence *in situ* hybridization (FISH). We focused initially on *Brn1* mRNA because it had widespread expression in RPs, as indicated by the scRNA-seq data (Figures 1A, 1B, and S1B), and because it is important for superficial layer neurogenesis (Sugitani et al., 2002; Dominguez et al., 2013). We analyzed the cortex at E12, before superficial layer neurons are generated. Immunostaining with an antibody that recognizes both Brn1 and Brn2 combined with FISH (Figures 2A and S2A) showed that Brn1/Brn2 protein was undetectable in the medial cortex, as published previously (Dominguez et al., 2013), but that *Brn1* mRNA was expressed in most Pax6-positive RPs. We asked whether these *Brn1* mRNA-positive RPs co-expressed other neuronal specification mRNAs, analyzing *Tle4* (layer V/VI), *Tle3* (layer II/III), and *Diap3* (predominantly layer V) mRNAs. Multi-label FISH at E12 and E13 showed that many RPs co-expressed these mRNAs and that about 70% of cells in the E13 precursor-containing ventricular zone (VZ) and subventricular zone (SVZ) co-expressed *Brn1*, *Tle4*, and *Diap3* mRNAs (Figures 2B–2D).

A similar analysis at E15 and E17 (Figures 2D–2F) showed that the proportion of VZ/SVZ cells co-expressing *Brn1*, *Tle4*, and *Diap3* mRNAs decreased from E13 to E17 but that approximately 30% of E17 RPs still co-expressed all 3 mRNAs. Coincidentally, there was an increase in VZ/SVZ cells that expressed only *Brn1* mRNA (Figure 2E). Triple-label FISH with negative control probes demonstrated the specificity of these analyses (Figures S2B and S2C).

We confirmed the co-expression of neuronal specification mRNAs in RPs by analyzing cultured E12.5 cortical precursors that generate neurons *in vitro*. Triple-label FISH combined with immunostaining (Figures 2G and 2H) showed that many βIII-tubulin-negative precursors co-expressed *Brn1*, *Tle4*, and *Diap3* mRNAs, although some were also positive only for *Brn1*

(C) Higher-resolution t-SNE visualizations of E15.5 RPs from the boxed regions in (A), showing overlaid expression of *Hes5*, *Brn1*, *Brn2*, *Tle3*, *Tle1*, *Pax6*, *Tle4*, *Ctip2*, *Fezf2*, and *Diap3* mRNAs. Gene expression levels are color-coded as in (A). Arrowheads denote individual RPs co-expressing superficial and deep layer specifier mRNAs.

(D) Table showing the percentage of E13.5, E15.5, and E17.5 RPs expressing both superficial and deep layer neuron specifiers, only superficial layer specifiers, or only deep layer specifiers.

(E) Histograms showing the number of specification mRNAs, of the 17 listed in (B), that were detected in individual RPs at E13.5, E15.5, and E17.5, expressed as a percentage of the total RPs at the same age.

(F) Average number of specification mRNAs detected in individual RPs at E13.5, E15.5, and E17.5. **$p < 0.01$, ***$p < 0.001$, ns = $p > 0.05$ by one-way ANOVA with Tukey's multiple comparisons test; n = 233, 273, and 77 RPs for E13.5, E15.5, and E17.5 respectively. Error bars denote SEM.

See also Figure S1.

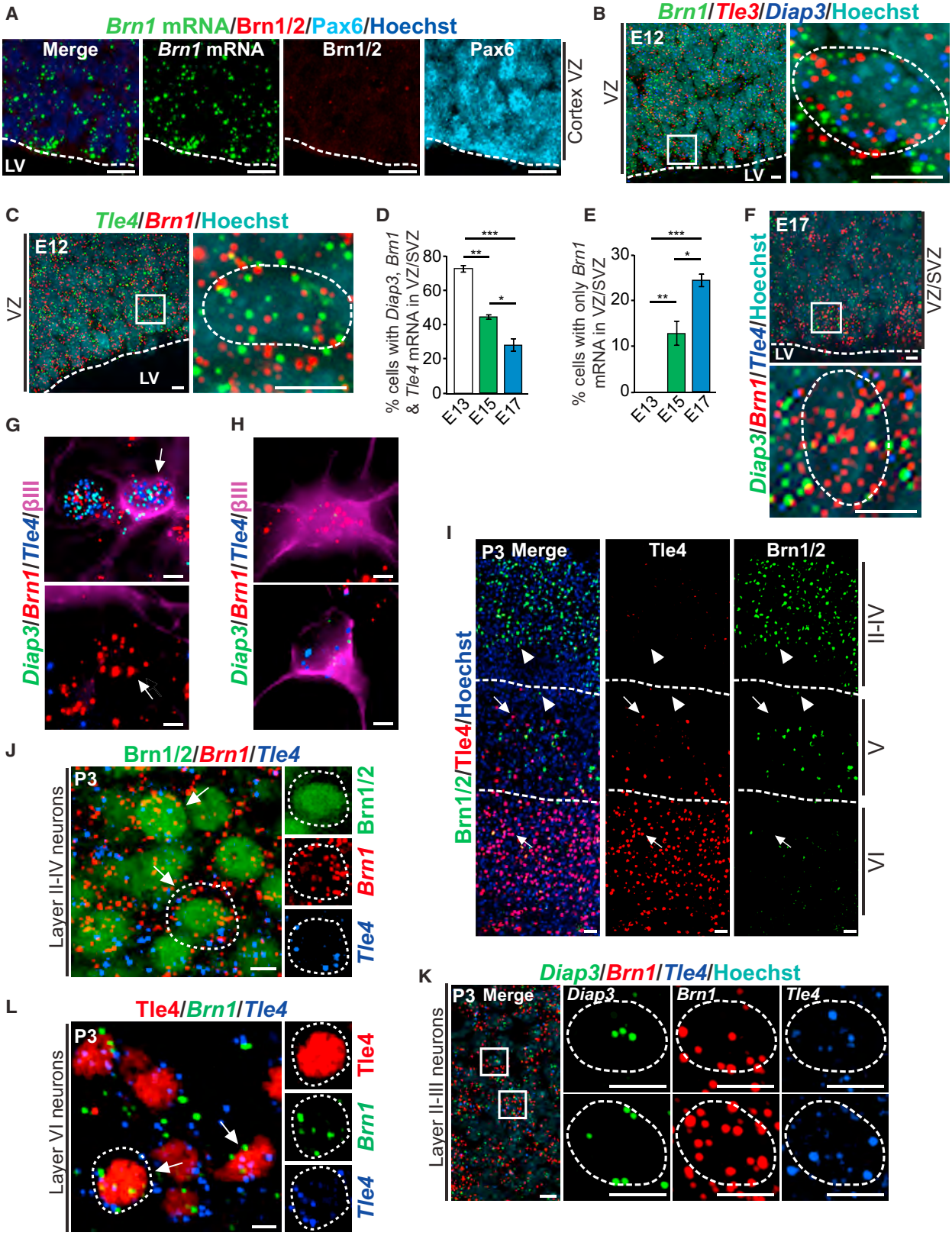

(legend on next page)

mRNA. Intriguingly, about 30% of newborn βIII-tubulin-positive neurons also co-expressed *Brn1*, *Tle4*, and *Diap3* mRNAs (Figure 2G, top), although many expressed only *Brn1* mRNA and some only *Tle4* mRNA (Figure 2H).

We asked whether this neuronal co-expression was also seen *in vivo*, examining the cortex at postnatal day 3 (P3), when neurogenesis is complete. Immunostaining (Figure 2I) confirmed that, as published previously (Yao et al., 1998; Dominguez et al., 2013), Brn1/2 and Tle4 proteins were detectably expressed in mutually exclusive superficial and deep layer neurons, respectively. In contrast, FISH showed that, in superficial layers II–IV, where there were no Tle4-positive cells, some Brn1/2 protein-positive cells expressed both *Brn1* and *Tle4* mRNAs (Figure 2J). Indeed, triple-label FISH showed that some neurons in the most superficial layers co-expressed *Brn1*, *Tle4*, and *Diap3* mRNAs (Figure 2K). Conversely, in layer VI, where there were no Brn1/2 protein-positive cells, some Tle4-protein positive cells co-expressed both *Tle4* and *Brn1* mRNAs (Figure 2L). Thus, newborn cortical neurons appropriately express laminar specification proteins, but, at the transcriptional level, some of them are more promiscuous.

Identification of a Pum2/4E-T Translational Repression Complex in Embryonic RPs

These data suggest that post-transcriptional regulation is important for neuronal specification. Because we showed that the translational repressor protein 4E-T regulates the extent and timing of cortical neurogenesis (Yang et al., 2014), we asked whether it might also be in a complex with neuronal specification mRNAs. Analysis of our previously published 4E-T RNA immunoprecipitation (RIP) data from the E12.5 cortex showed that *Brn1*, *Tle3*, *Tle4*, *Mef2c*, *Bhlhe22*, and *Diap3* mRNAs were all significantly associated with 4E-T (adjusted p values: *Brn1*, 1.75×10^{-3}; *Tle3*, 8.53×10^{-4}; *Tle4*, 2.81×10^{-3}; *Mef2c*, 1.55×10^{-3}; *Bhlhe22*, 2.72×10^{-6}; *Diap3*, 6.13×10^{-2}). We confirmed the association of 4E-T with *Brn1*, *Tle3*, and *Tle4* mRNAs in the RIPs by performing qPCR analysis (Figure 3A).

Because 4E-T does not directly bind RNA, we asked whether the 3′ UTRs of cortical mRNAs associated with 4E-T were enriched in RNA-binding protein consensus elements, as predicted by RNAcompete (Ray et al., 2009). This analysis showed that Pumilio1/2 (Pum1/2) consensus motifs significantly distinguished 4E-T target mRNAs from background mRNAs (area under the receiver operating characteristic curve [AU-ROC] = 0.79; STAR Methods). Of particular relevance is that *Brn1*, *Tle3*, *Tle4*, *Bhlhe22*, *Diap3*, and *Mef2c* mRNAs all had computationally predicted Pum1/2 consensus sites (Table S1).

Because Pumilio proteins are known translational repressors (Wickens et al., 2002; Miller and Olivas, 2011; Quenault et al., 2011), and Pum2 is expressed in embryonic cortical RPs (Vessey et al., 2012), we asked whether Pum2 and 4E-T were associated in the embryonic cortex. Four lines of evidence indicated that they were. First, western blots showed that Pum2 was present in anti-4E-T immunoprecipitated complexes from the E12/13 cortex (Figure 3B). Second, immunostaining of cultured E12/13 cortical precursors showed that Pum2 and 4E-T were both present in cytoplasmic granule-like structures and that about 65% of Pum2-positive puncta were also positive for 4E-T (Figure 3C). Moreover, as seen previously for 4E-T (Yang et al., 2014), many Pum2-positive puncta were also positive for the P body protein

Figure 2. Developing Cortical RPs and Newborn Neurons Co-express mRNAs Associated with Superficial and Deep Layer Cortical Neurons

(A) Representative high-magnification confocal z stack images of the E12 cortical VZ showing FISH for *Brn1* mRNA (green, left and center left) and immunostaining for Pax6 (turquoise, right) and Brn1/2 protein (red, center right; not detectable at this age). The merged image (left) shows Brn1/2 protein, *Brn1* mRNA, and Hoechst 33258 counterstain (dark blue), but not Pax6. The hatched white lines denote the apical cortical border with the lateral ventricle (LV). A corresponding low-magnification image of the same section is shown in Figure S2A.

(B and C) Representative confocal z stack images of multi-label FISH for *Brn1* (green), *Tle3* (red), and *Diap3* (blue) (B) or *Brn1* (red) and *Tle4* (green) (C) mRNAs in E12 coronal cortical sections, showing the VZ and the apical border (hatched white line). The boxed areas are also shown at higher magnification at the right, and single-cell nuclei are highlighted (outlined in white; Hoechst counterstain is light blue).

(D and E) Quantification of images as in (B), (C), and (F) for the proportion of VZ/SVZ cells expressing *Brn1*, *Diap3*, and *Tle4* mRNAs (D) or *Brn1* mRNA only (E) at E13, E15, and E17. *$p < 0.05$, **$p < 0.01$, ***$p < 0.001$; n = 3 embryos per time point, 100 cells per embryo.

(F) Representative confocal z stack image of multi-label FISH for *Brn1* (red), *Tle4* (blue), and *Diap3* (green) mRNAs in an E17 coronal cortical section, showing the VZ/SVZ and the apical border (hatched white line). The boxed area is also shown at higher magnification at the bottom, and a single cell nucleus is highlighted (outlined in white; Hoechst counterstain is light blue).

(G and H) Representative z stack images of cortical cultures immunostained for ßIII-tubulin (purple) and analyzed by FISH for *Brn1* (red), *Tle4* (blue), and *Diap3* (green) mRNAs. The arrow in the top image in (G) denotes a ßIII-tubulin-positive cell co-expressing all three mRNAs, whereas the arrow in the lower image (G) denotes a ßIII-tubulin-negative cell expressing only *Brn1* mRNA.

(I) Representative images of a P3 cortical section immunostained for Brn1/2 (green) and Tle4 (red) and counterstained with Hoechst 33258 (blue in the left merged image). Arrows and arrowheads denote Tle4-positive and Brn1/2-positive neurons, respectively. Hatched lines delineate boundaries between layers II–IV, V, and VI.

(J) High-magnification confocal image showing FISH for *Brn1* (red) and *Tle4* (blue) mRNAs and immunostaining for Brn1/2 (green) in the superficial layers (II–IV) of the P3 cortex. Arrows indicate neurons co-expressing *Brn1* and *Tle4* mRNAs, and one of these (circled) is shown at higher magnification at the right, with the color channels pulled apart.

(K) Representative confocal z stack images showing FISH for *Brn1* (red), *Tle4* (blue), and *Diap3* (green) mRNAs in the superficial layers (II/III) of the P3 cortex. Boxed cells are shown at higher magnification on the right, with the color channels pulled apart. White ovals denote cell boundaries defined by Hoechst nuclear staining (light blue/gray in the left merged image).

(L) High-magnification confocal image showing FISH for *Brn1* (green) and *Tle4* (blue) mRNAs and immunostaining for Tle4 (red) in layer VI of the P3 cortex. Arrows denote neurons co-expressing *Brn1* and *Tle4* mRNAs, and one of these (circled) is shown at higher magnification on the right, with the color channels shown separately.

Scale bars, 10 μm in (A) and (K) (low magnification), 5 μm in (B), (C), (F)–(H), (J), (L), and (K) (high magnification), and 30 μm in (I). Error bars denote SEM. See also Figure S2.

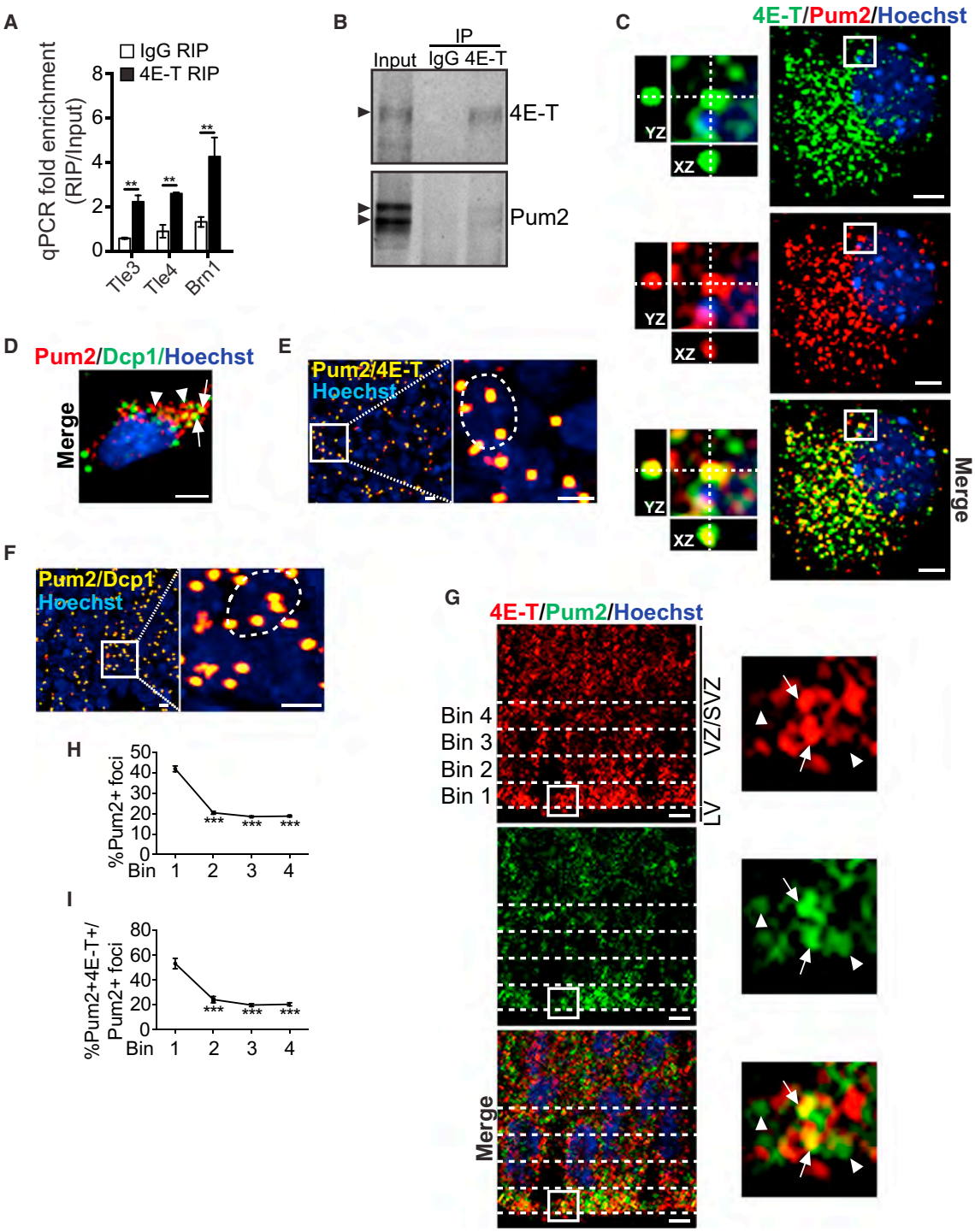

Figure 3. Pum2 and 4E-T Are Closely Associated in Embryonic RPs

(A) qPCR validation for *Tle3*, *Tle4*, and *Brn1* mRNAs in three independent 4E-T and control IgG immunoprecipitates and their initial inputs. Shown is fold enrichment of each mRNA relative to input. **p < 0.01 (pairwise comparison to IgG RIP).

(B) Western blots of E12.5 cortical lysates (input) immunoprecipitated with control IgG (IgG) or anti-4E-T (4E-T), probed for 4E-T or Pum2. Arrowheads denote target proteins.

(C and D) Representative images of E12 precursors cultured for 3 days, immunostained for Pum2 (red) and 4E-T (green, C) or Dcp1 (green, D), and counterstained with Hoechst 33258 (blue). The boxed regions in (C) are shown at higher magnification (left) and also indicate co-localization on the z axis (XZ and YZ) with hatched lines. In (D), arrows and arrowheads indicate Pum2 foci positive or negative for Dcp1, respectively.

(legend continued on next page)

Dcp1 (Figure 3D). Third, proximity ligation assays identified foci in cultured cortical precursors where Pum2 was located within 40 nm of 4E-T or Dcp1 (Figures 3E and 3F). In contrast, proximity ligation assays for Pum2 and the NPY1 receptor or Pax6 showed only a few background dots (Figure S3).

Fourth, we asked whether Pum2 and 4E-T were associated *in vivo*. Immunostaining of E13 cortical sections (Figure 3G) showed that Pum2-positive puncta were present throughout the cortex and significantly enriched in the most apical region of the VZ (Figures 3G and 3H). In this same apical region, about 50% of Pum2-positive puncta were also positive for 4E-T (Figures 3G and 3I). To ensure that this co-localization was specific, we randomized the images (Costes et al., 2004). For the original Pum2/4E-T data, Pearson's coefficient was r = 0.541, and for the randomized data it was r = 0.0 ± 0.009 (p = 100% that co-localization was not random).

Pum2 and 4E-T Share Target mRNAs, Including Neuronal Specification mRNAs

These data predict that some 4E-T target mRNAs would be associated with Pum2. To test this prediction, we immunoprecipitated Pum2 from the E12 cortex and analyzed the co-immunoprecipitated mRNAs by microarrays (GEO: GSE108404). As controls, we performed similar immunoprecipitations with non-specific immunoglobulin G (IgG). We analyzed these microarray datasets (three independent replicates each of the Pum2 and IgG immunoprecipitations), first removing all non-protein-coding genes and genes with an IgG/input fold change of greater than 1.5. We then defined the Pum2 target set as those remaining mRNAs that were enriched more than 1.5-fold in the Pum2 RIP versus input, with $p < 0.05$. We also defined a background set, including mRNAs that were not enriched in the Pum2 RIP (fold change of less than 1) with $p < 0.05$. This analysis defined 1,783 probes as Pum2 targets and 2,806 as the background set (Table S2). Of the 1,783 Pum2 target mRNAs, 282 were also 4E-T target mRNAs that had Pum1/2 consensus motifs in their 3′ UTRs (Table S1), including *Tle3*, *Tle4*, *Neurog1*, *Neurog2*, *Ascl1*, and *Mef2c* mRNAs. *Brn1* mRNA, which is a 4E-T target that contains consensus Pum1/2 motifs (Table S1), was also significantly associated with Pum2 in the RIP dataset (p = 0.017) but was enriched only 1.3-fold. Other mRNAs defined as shared Pum2 and 4E-T targets that encoded transcriptional regulators were *Arid1a*, *Bcl6*, *Ets2*, *E2f3*, *Gli2*, *Klf6*, *Mkl1*, *Meis1*, *Nkrf*, *Phf12*, *Pou3f4*, *Prdm16*, *Sox13*, *Sox2*, *Rere*, *Bhlhe40*, *Cbx4*, *Cbx8*, *Elp3*, *Epc2*, *Foxc1*, *Foxk1*, *Irf2bp1*, *Jun*, *Lin54*, *Maml1*, *Med23*, *Mn1*, *Myc*, *Mef2a*, *Nrip1*, *Nfya*, *Pias1*, *Rnf44*, *Sal13*, *Stat3*, *Six4*, *Txnip*, *Sp8*, *Tfap2a*, *Usp22*, *Mafb*, *Mycn*, *Zbtb14*, *Zfp11*, *Zfp143*, *Zfp229*, *Zfp273*, *Zfp282*, *Zfp518a*, *Zfp763*, *Zfp85*, *Zic1*, *Zic3*, and *Zhx1*.

We validated the Pum2 RIP dataset in a number of ways. First, computational analysis defined significantly more Pum1/2 motif occurrences in the 3′ UTRs of Pum2 target mRNAs versus a set of background mRNAs not enriched in the Pum2 RIP (Figure 4A). Second, qPCR of three independent Pum2 RIP experiments confirmed that *Tle3*, *Tle4*, *Brn1*, *Neurog1*, and *Neurog2* mRNAs were all significantly enriched in the Pum2 RIPs (Figure 4B). Finally, we performed a correlation analysis, comparing relative fold changes in mRNA levels as determined by microarrays versus qPCRs. For this comparison, we analyzed the shared Pum2 and 4E-T target mRNAs (*Tle3*, *Tle4*, *Brn1*, *Neurog1*, and *Neurog2*) and eight other Pum2 target mRNAs (*4et*, *Brn4*, *Prox1*, *Celsr2*, *Foxq1*, *Ptpru*, *Rabgef1*, and *Tspan14*). We also included four mRNAs (*Foxf2*, *Sepp1*, *Cox6b1*, and *Mmd2*) that were not enriched in the Pum2 RIPs. There was an excellent correlation (r = 0.918) between the fold changes obtained using microarrays versus qPCRs (Figure 4C).

We next used the database for annotation, visualization, and integrated discovery (DAVID) to perform gene ontology on all Pum2 target mRNAs in the RIP dataset and on the subset of these that were also 4E-T target mRNAs. Total Pum2 targets were highly enriched for proteins associated with cell adhesion, cell migration, transcription, cell differentiation, cell cycle and forebrain, projection neuron, and stem cell development (Figure 4D; Table S3). The Pum2/4E-T shared targets were particularly enriched for proteins associated with transcriptional regulation and nervous system/neuronal development (Figure 4E; Table S3). We obtained a similar enrichment for transcriptional regulators when the Pum2/4E-T dataset was analyzed by protein analysis through evolutionary relationships (PANTHER). Of 282 shared target mRNAs, 126 encoded proteins assigned to categories by PANTHER, and the most enriched group included 37 transcription factors (Table S4).

Pum2 and 4E-T Are Associated with Brn1 and Tle4 mRNAs in Apical RPs during Cortical Neurogenesis

The shared Pum2 and 4E-T transcription factor targets included *Brn1* and *Tle4* mRNAs. Because these mRNAs are co-expressed during neurogenesis, we asked whether they were associated with Pum2 and/or 4E-T in RPs. Initially, we used immunostaining and FISH to define their expression patterns in the E12 cortex during deep layer neurogenesis. At this age, 4E-T and Pum2 proteins were detectable throughout the cortex (Figure 4F). Brn1 protein was not detectable, but *Brn1* mRNA was present in all cortical layers (Figure 4F), in agreement with the E13.5 scRNA-seq data (Figure S1B), which also showed that the

(E and F) Representative confocal z stack images of E12 precursors cultured for 3 days and analyzed by proximity litigation assay (PLA) with antibodies for Pum2 and 4E-T (E) or Dcp1 (F). Cells were counterstained with Hoechst 33258 (blue), and gold dots indicate the PLA signal. Boxed regions are expanded on the right, and single nuclei are demarcated (hatched lines).

(G) Confocal images of an E13 section immunostained for Pum2 (green) and 4E-T (red), counterstained with Hoechst 33258 (blue in merged image). Boxed regions are expanded on the right. Arrows and arrowheads denote Pum2 foci that are or are not co-localized with 4E-T. Hatched white lines denote the four bins used for quantification.

(H and I) Quantification of the images as in (G) for the percentage of total Pum2 granules in each of the four bins (H) or for the percentages of Pum2 granules in each bin that were also positive for 4E-T (I). ***$p < 0.001$ by one-way ANOVA with Dunnett's multiple comparisons test; n = 3 embryos.

Scale bars, 5 μm. Error bars denote SEM. See also Figure S3.

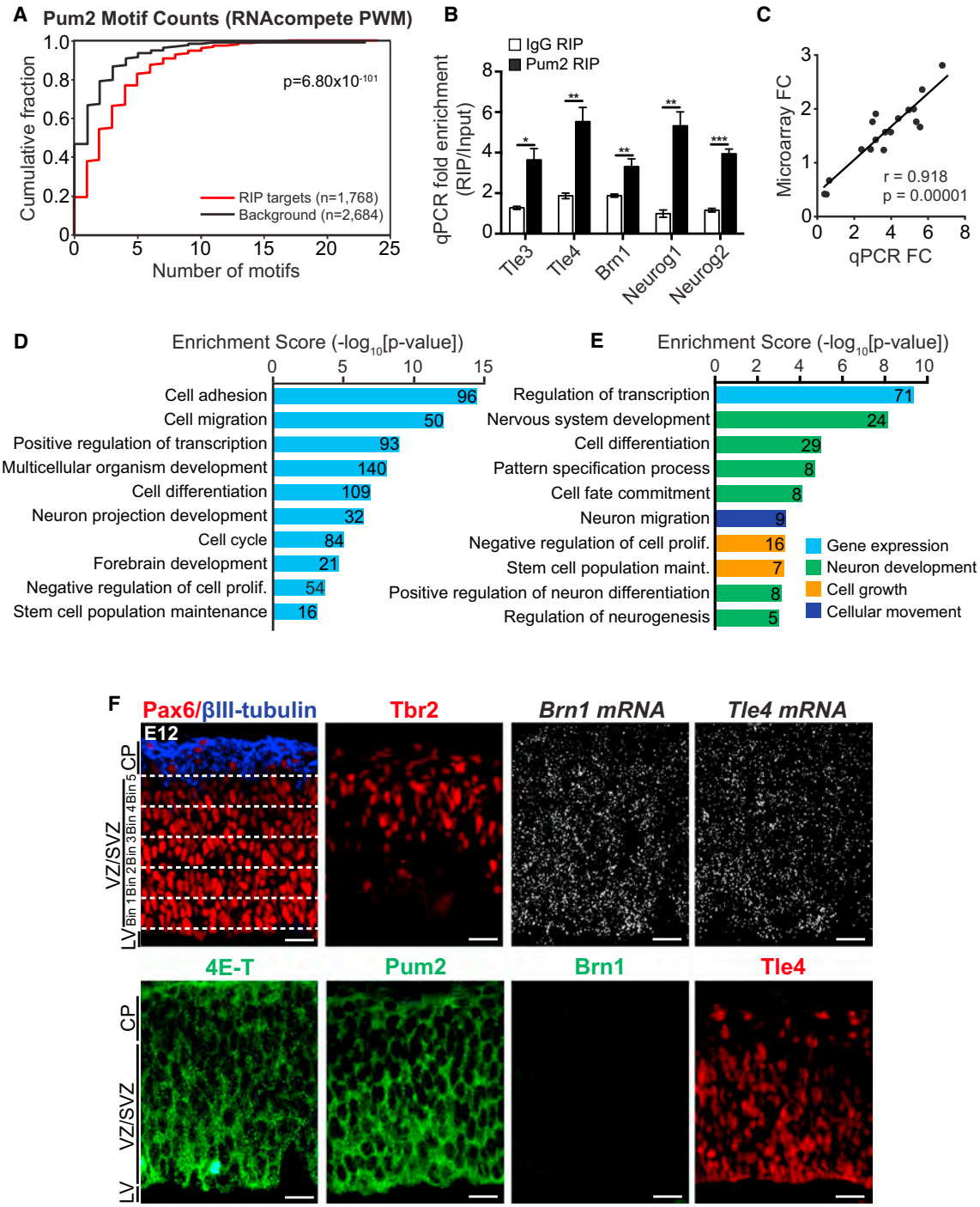

Figure 4. Pum2 and 4E-T Share Target mRNAs

(A–E) Pum2 was immunoprecipitated from the E12/E13 cortex, and associated mRNAs were analyzed by microarray (GEO: GSE108404). As a control, similar immunoprecipitations were performed with non-specific IgG. Three independent samples of each were analyzed. The Pum2 target set was defined as the 1,768 mRNAs with enrichment of greater than 1.5-fold ($p < 0.05$) versus the input, whereas the background set included 2,684 mRNAs that were not enriched in the Pum2 RIP (fold change of less than 1; $p < 0.05$) (see Table S2 for lists of these mRNAs).

(A) The 3′ UTRs of mRNAs from the Pum2 RIP target and background datasets were analyzed for occurrences of the top 10 Pum1/2 n-mer consensus motifs predicted by the RNAcompete position frequency matrix (PFM). Motif occurrences were counted, and the cumulative distribution function (CDF) of motif counts is displayed separately for the two groups of mRNAs. The CDF calculates the cumulative probability for a given motif count, and this is significantly larger in the target versus background datasets ($p = 6.80 \times 10^{-101}$, Wilcoxon rank-sum test).

(legend continued on next page)

average *Brn1* mRNA levels in *Brn1*-positive RPs and neurons were similar (1.34 and 1.38 a.u., respectively). In contrast to Brn1, at E12, Tle4 protein was present in cells from the VZ/SVZ to the cortical plate (CP) (Figure 4F), consistent with ongoing deep layer neurogenesis. *Tle4* mRNA was also distributed across the E12 cortex (Figure 4F), in agreement with the E13.5 scRNA-seq, showing similar expression levels in *Tle4*-positive RPs and neurons (0.97 and 1.33 a.u., respectively). As controls for the specificity of the FISH, we showed that two RP markers, *Vcam1* and *Aldoc* mRNAs, were found only in the VZ/SVZ of the E13 cortex (Figure S4A).

We next performed co-localization studies, combining immunostaining and FISH. Quantification of *Brn1* mRNA in the CP and five equal-sized bins spanning the VZ/SVZ confirmed that it was equally distributed across the cortex (Figures 4F, 5A, and 5C). Approximately half of the *Brn1* mRNA foci were co-localized with 4E-T in the most apical precursors (Bin 1) and in the CP, with significantly less co-localization in other regions (Figures 5A and 5D). A similar high level of co-localization between Pum2 and *Brn1* mRNA was found in the most apical RPs (Figures 5B and 5E), with 30%–40% co-localization in other cortical compartments. A similar analysis for *Tle4* mRNA confirmed that it was also equally distributed across the cortex (Figures 4F, 5F, and 5H). However, only about 20% of *Tle4* mRNA was associated with 4E-T in the most apical RPs (Bin 1), with less association elsewhere (Figures 5F and 5I). Co-localization with Pum2 was also lower, with approximately 29% of *Tle4* mRNA foci associated with Pum2 in the VZ and less elsewhere (Figures 5G and 5J).

Two controls demonstrated the specificity of these analyses. First, we randomized the data (Costes et al., 2004). For the original versus randomized 4E-T/*Brn1* mRNA data, Pearson's coefficients were r = 0.271 and r = 0.0 ± 0.033, respectively (p = 100%). For the original versus randomized 4E-T/*Tle4* mRNA data, r = 0.198 and r = 0.0 ± 0.057 (p = 100%). For the original versus randomized Pum2/*Brn1* mRNA data, r = 0.465 and r = 0.0 ± 0.038 (p = 100%). For the original versus randomized Pum2/*Tle4* mRNA data, r = 0.357 and r = 0.0 ± 0.008 (p = 100%). Second, we performed a co-localization analysis for *Glo1* mRNA, which is not a target of Pum2 or 4E-T. Less than 19% of *Glo1* mRNA foci were co-localized with Pum2 in the E12 VZ/SVZ (Figures S4B and S4C), and our previously published data showed a similar low level of co-localization (10%–13%) of *Glo1* mRNA with 4E-T in the VZ/SVZ (Yang et al., 2014). Thus, both *Brn1* and *Tle4* mRNAs co-localize with 4E-T and Pum2 in E12 apical RPs, but *Brn1* mRNA is more highly co-localized.

These data showed that about 50% of *Brn1* mRNA was associated with 4E-T in E12 apical RPs. We asked whether this was also true at E16 during superficial layer neurogenesis. As seen at E12, 4E-T and Pum2 proteins and *Brn1* mRNA were all expressed throughout the cortex (Figures 5L, S4D, and S4E). However, at this age, Brn1 protein was also readily detectable in cells located from the SVZ to the CP (Figure S4D), as published previously (Dominguez et al., 2013). Quantification showed that *Brn1* mRNA was equally distributed across the VZ/SVZ and that it was co-localized with 4E-T in the most apical RPs but that the association with 4E-T was significantly decreased relative to E12 by more than 2-fold (Figures 5K–5N). Thus, translation of Brn1 protein during superficial layer neurogenesis is associated with a decreased association between *Brn1* mRNA and 4E-T in RPs.

Pum2 or 4E-T Knockdown Causes Aberrant Co-expression of Brn1 and Tle4 Proteins during Neurogenesis

These data suggest that a Pum2/4E-T complex selectively represses mRNAs to regulate cortical neurogenesis and neuronal specification. In this regard, we showed previously that 4E-T knockdown enhanced neurogenesis by derepressing basic-helix-loop-helix (bHLH) proneurogenic mRNAs (Yang et al., 2014). Because our RIP data indicated that *Ascl1*, *Neurog1*, and *Neurog2* were also Pum2 targets, we asked whether Pum2 regulated neurogenesis by knocking it down with a previously characterized Pum2 short hairpin RNA (shRNA) (Vessey et al., 2006, 2010) after confirming its efficacy in cultured cortical precursors (Figures S5A and S5B). Specifically, we electroporated E13/14 cortices with Pum2 shRNA and a nuclear EGFP plasmid, selectively transducing RPs that generate predominantly (90%) superficial layer neurons (Tsui et al., 2013; Gallagher et al., 2015). Immunostaining 3 days later demonstrated that EGFP-positive cell locations were altered by Pum2 knockdown, with a lower proportion in the VZ and CP and a higher proportion in the SVZ (Figures 6A and 6B).

We asked whether these alterations reflected aberrant neurogenesis by immunostaining for EGFP and the RP marker Pax6, the proliferation marker Ki67, or the IP marker Tbr2 (Figures 6C and S5C). Pum2 knockdown significantly decreased the proportions of EGFP-positive RPs and proliferating precursors and increased EGFP-positive, Tbr2-positive IPs (Figures 6D–6F). These alterations were not due to increased cell death because

(B) qPCR validation of *Brn1*, *Tle3*, *Tle4*, *Neurog1*, and *Neurog2* mRNAs in three independent Pum2 and control IgG immunoprecipitates and their initial inputs. Shown is fold enrichment of each mRNA relative to input. *p < 0.05, **p < 0.01, ***p < 0.001 (pairwise comparison with IgG RIP).

(C) Correlation of the average fold change (immunoprecipitates/input, n = 3) in the Pum2 RIP microarray versus qPCR analyses for the shared Pum2/4E-T target mRNAs in (B), eight other Pum2 target mRNAs (*4et*, *Prox1*, *Brn4*, *Celsr2*, *Foxq1*, *Ptpru*, *Rabgef1*, and *Tspan14*), and four mRNAs that were not enriched in the Pum2 RIPs (*Foxf2*, *Sepp1*, *Cox6b1*, and *Mmd2*). Each point represents one of these mRNAs. Pearson's correlation coefficient = 0.918, p = 0.00001.

(D and E) Gene ontology and pathway analysis for all Pum2 target mRNAs in the E12/E13 cortex (Tables S2 and S3) (D) and for the 282 shared Pum2 and 4E-T target mRNAs (Tables S1 and S3) (E). Shown are the top ontology terms ranked by their enrichment score (−log10 [p value], x axis; determined by a modified Fisher's exact test) and the number of genes in each category. In (E), the terms were classified into four color-coded groups based on their biological functions. Some genes are annotated in several categories.

(F) Confocal images of E12 medial cortex sections immunostained for 4E-T (green), Pum2 (green), Brn1 (green, not detectable at this age), and Tle4 (red) or analyzed by FISH for *Brn1* or *Tle4* mRNA (both white dots). Also shown is immunostaining for Pax6 (red), Tbr2 (red), and βIII-tubulin (blue) to define the VZ, SVZ, and CP, respectively. The top left shows the 5 VZ/SVZ bins used for quantification. Scale bars, 30 μm.

Error bars denote SEM.

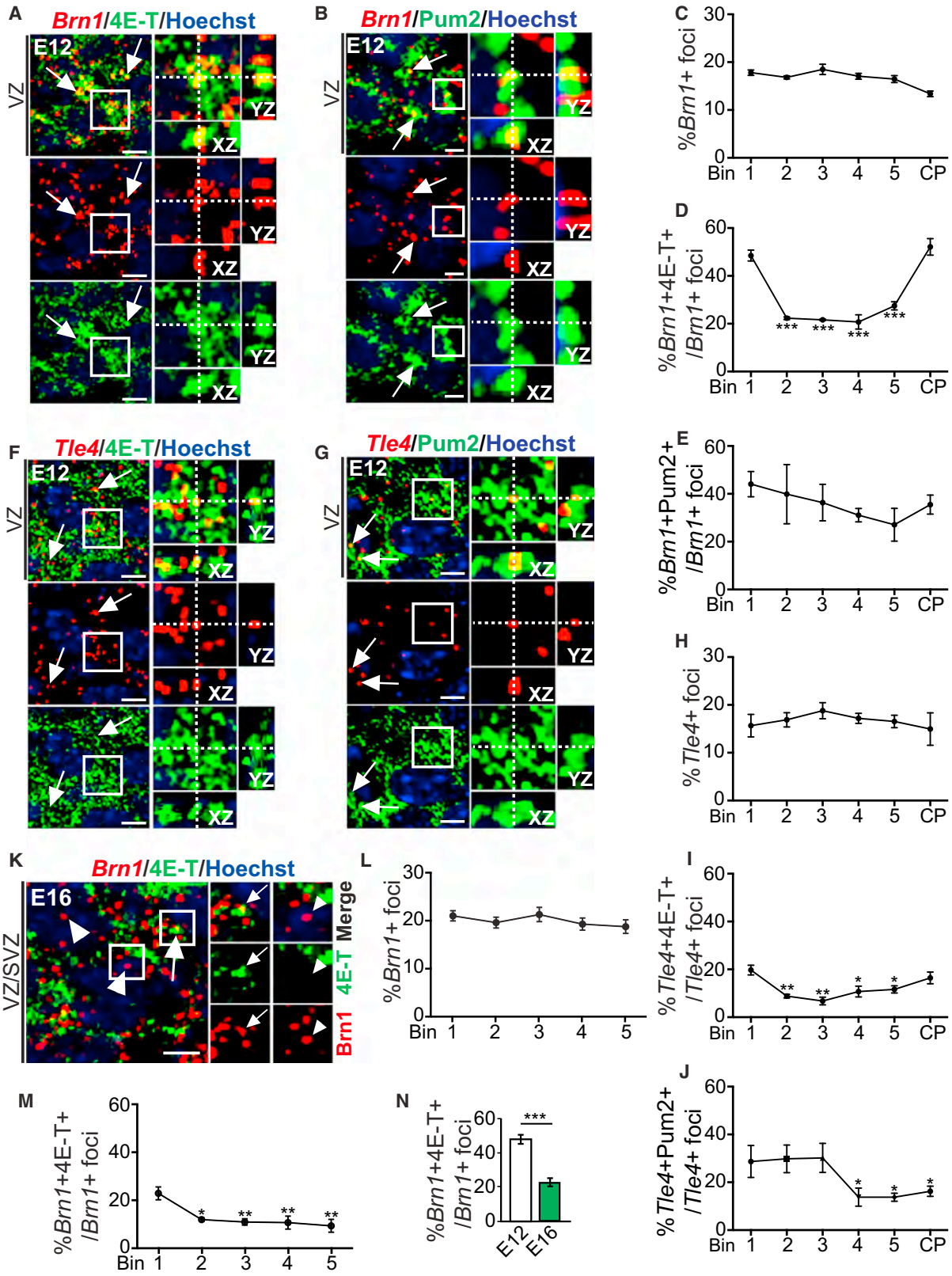

(legend on next page)

three or fewer EGFP-positive cells per section expressed the apoptotic marker cleaved caspase-3 2 days post-electroporation with either control or Pum2 shRNA (n = 3 embryos each). Thus, like 4E-T knockdown, Pum2 knockdown enhanced neurogenesis.

To ask whether Pum2 knockdown also affected neuronal specification, we performed similar electroporations and analyzed Brn1 and Tle4 protein expression. Immunostaining 3 days post-electroporation showed that, in controls, approximately 77% and 6% of EGFP-positive cells expressed Brn1 and Tle4 proteins, respectively (Figures 6G–6I). Pum2 knockdown had no effect on Brn1-positive cells but significantly increased EGFP-positive, Tle4-positive cells by about 3-fold (Figures 6H and 6I). Almost all EGFP-positive, Tle4-positive cells were also positive for Brn1 protein (Figures 6G and 6J). The large majority of these triple-labeled cells were located outside of the VZ, with most in the intermediate zone or CP (Figures 6G and 6J). Thus, Pum2 knockdown caused aberrant Tle4 protein expression in Brn1 protein-positive cells, predominantly superficial neurons.

We asked whether 4E-T knockdown had similar effects using a previously characterized 4E-T shRNA (Yang et al., 2014). Three days post-electroporation with either control or 4E-T shRNAs, approximately 80% of EGFP-positive cells were Brn1 positive (Figures 7A and 7B). However, the proportion of Tle4-positive cells was almost tripled by 4E-T knockdown, and almost all of these Tle4 protein-positive cells co-expressed Brn1 protein (Figures 7A, 7C, and 7D).

Several additional experiments argued that the aberrant co-expression of Tle4 in Brn1-positive cells was not simply due to enhanced neurogenesis. First, we performed similar electroporations with an expression plasmid for Creb binding protein (CBP) S436D, an activated CBP phosphomimic that enhances neurogenesis by regulating histone acetylation (Wang et al., 2010, 2012). As predicted, CBP S436D enhanced neurogenesis, as indicated by an increase in EGFP-positive cells in the CP and a decrease in the VZ (Figure 7E). It did not, however, alter the proportion of EGFP-positive cells expressing Brn1 protein, Tle4 protein, or both (Figures 7F and 7G). Second, we transfected cultured E11.5 cortical precursors with Pum2, 4E-T, or control shRNA and a nuclear EGFP plasmid. Immunostaining 2 days later showed that Pum2 or 4E-T knockdown increased the proportion of EGFP-positive, βIII-tubulin-negative precursors that co-expressed Tle4 and Brn1/2 proteins (Figures S6A and S6B). Finally, we performed E13/14 electroporations with control, Pum2, or 4E-T shRNA and analyzed them at 2 rather than 3 days, at which time point half of the electroporated cells are RPs and a further 20%–25% IPs (Yuzwa et al., 2016; Figures S6C and S6D). In controls, approximately 65%–70% of EGFP-positive VZ/SVZ cells were Brn1 protein positive, and this did not change with Pum2 or 4E-T knockdown (Figures 7H, S6E, and S6F). In contrast, Pum2 or 4E-T knockdown caused an approximately 3-fold increase in EGFP-positive, Tle4 protein-positive VZ/SVZ cells, and almost all of these were also positive for Brn1 protein (Figures 7I and 7J). Thus, Pum2 or 4E-T knockdown caused aberrant co-expression of Brn1 and Tle4 proteins in both precursors and newborn neurons.

Disruption of Pum2 or 4E-T Derepresses a Deep Layer Neuron Phenotype in Newborn Superficial Layer Neurons

We next asked whether the aberrant co-expression of Tle4 in Brn1-positive cells reflected a general derepression of a deep layer neuron phenotype by immunostaining electroporated sections for Brn1 and three other deep layer transcription factors, Ctip2, Tbr1, and FoxP2 (Figures 8A, 8B, and S7). In controls, 72% of EGFP-positive cells were Brn1 protein positive, and very few expressed Ctip2 (1%), Tbr1 (4%–5%), or FoxP2 (6%–7%) proteins (Figures 8A–8D, 8F, 8H, and S7). Following Pum2 knockdown, EGFP-positive, Brn1 protein-positive cells were unaltered, but EGFP-positive cells expressing Ctip2, Tbr1, or FoxP2 were increased to more than 15% (Figures 8A–8D, 8F, 8H, and Figure S7), and almost all of these were also positive

Figure 5. Cortical Neuron Specification mRNAs Are Associated with 4E-T and Pum2 in Embryonic RPs

(A and B) Confocal images showing FISH for *Brn1* mRNA (red) and immunostaining for 4E-T (green; A) or Pum2 (green; B) in the E12 VZ. Sections were counterstained with Hoechst 33258 (blue). Arrows denote co-localized foci. Shown on the right are higher-magnification images of the boxed regions that also show co-localization on the z axis (XZ and YZ, indicated by hatched white lines).

(C–E) The E12 VZ/SVZ was divided into five equal bins, and the CP was considered as a separate bin (Figure 4F). Sections as in (A) and (B) were then quantified for the percentage of total *Brn1* mRNA foci in each bin (C) or for the percentages of *Brn1* mRNA foci within a bin that were co-localized with 4E-T (D) or Pum2 (E). ***$p < 0.001$ by one-way ANOVA with Dunnett's multiple comparisons test; n = 3 embryos each.

(F and G) Confocal images showing FISH for *Tle4* mRNA (red) and immunostaining for 4E-T (green; F) or Pum2 (green; G) in the E12 VZ. Sections were counterstained with Hoechst 33258 (blue). Arrows denote co-localized foci. Shown on the right are high-magnification images of the boxed regions that also show co-localization on the z axis (XZ and YZ, indicated by hatched white lines).

(H–J) The E12 cortex was subdivided as in (C)–(E), and sections as in (F) and (G) were then quantified for the percentage of total *Tle4* mRNA foci in each bin (H) or for the percentages of *Tle4* mRNA foci within a bin that were co-localized with 4E-T (I) or Pum2 (J). *$p < 0.05$, **$p < 0.01$ by one-way ANOVA with Dunnett's multiple comparisons test; n = 3 embryos each.

(K) Confocal image showing FISH for *Brn1* (red) and immunostaining of 4E-T (green) in the E16 VZ. The section was counterstained with Hoechst 33258 (blue). The boxed regions are expanded on the right, where the color channels are separated. Arrows denote *Brn1*-positive, 4E-T-positive foci and arrowheads foci that are *Brn1* positive only.

(L and M) The E16 VZ/SVZ was divided into five bins of equal width and quantified for the percentage of total *Brn1* mRNA-positive foci in each bin (L) or for the percentages of *Brn1* mRNA-positive foci within a bin that were co-localized with 4E-T (M). *$p < 0.05$, **$p < 0.01$ by one-way ANOVA with Dunnett's multiple comparisons test; n = 3 embryos each.

(N) Quantification of the percentages of *Brn1* mRNA-positive foci in the most apical bin (Bin 1) that were co-localized with 4E-T at E12 (white bar) and E16 (green bar). ***$p < 0.001$; n = 3 embryos each.

Scale bars, 5 μm. Error bars denote SEM. See also Figure S4.

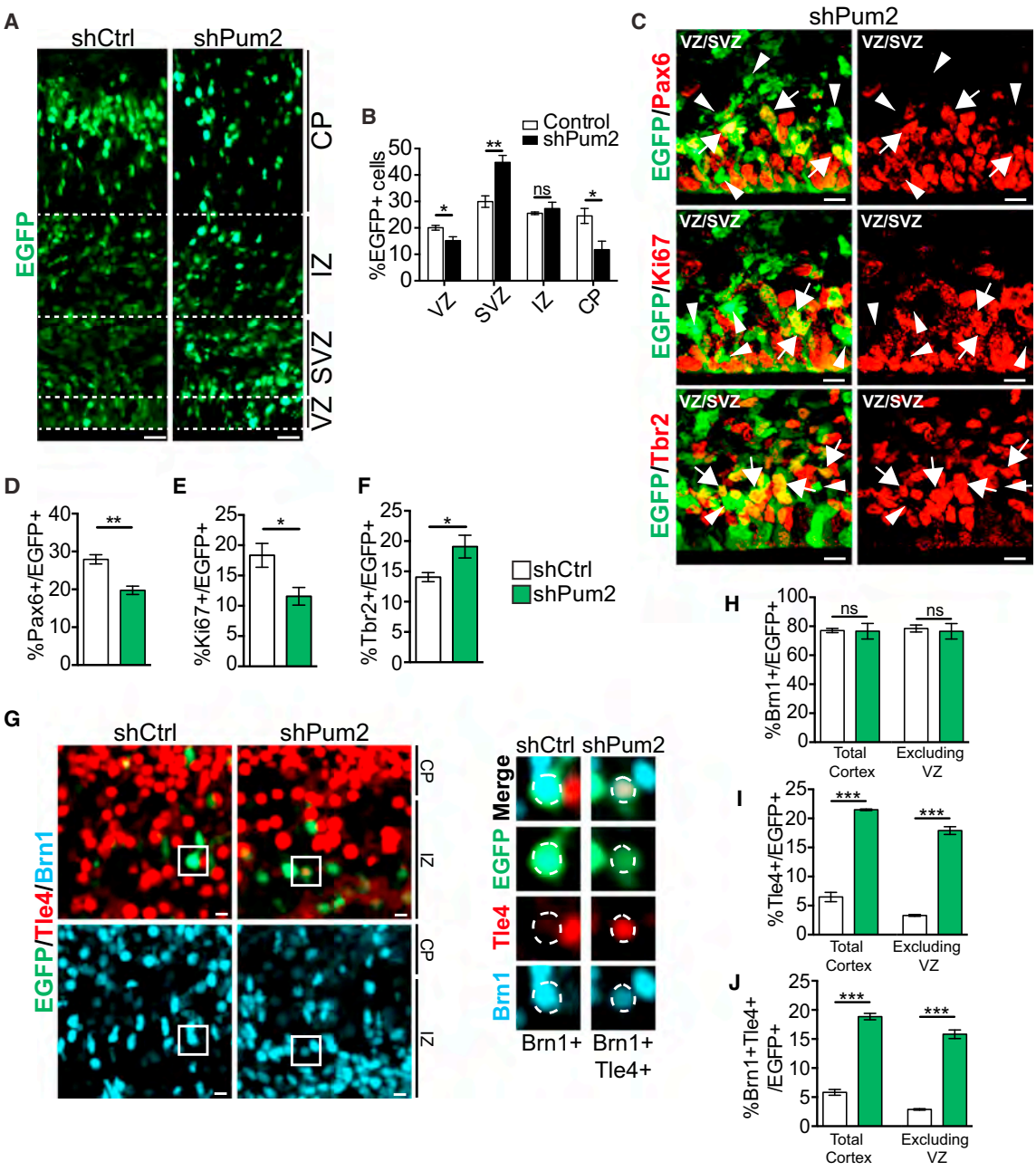

Figure 6. Pum2 Is Important for Regulating Neurogenesis and Neuronal Specification

E13/E14 cortices were electroporated with a nuclear EGFP plasmid and Pum2 (shPum2) or control (shCtrl) shRNA, and coronal cortical sections were immunostained 3 days later at E16/E17.

(A) Representative images of electroporated sections immunostained for EGFP. Hatched white lines delineate the borders of the cortical regions. IZ, intermediate zone.

(B) Quantification of images as in (A) for the percentages of EGFP-positive cells in each of the cortical regions. *$p < 0.05$, **$p < 0.01$; $n = 4$ embryos each, 3–4 sections per embryo.

(C) Representative confocal z stack images of the VZ/SVZ of sections electroporated with Pum2 shRNA and immunostained for EGFP (green) and Pax6 (red, top), Ki67 (red, center), or Tbr2 (red, bottom). Arrows and arrowheads indicate EGFP-positive, marker-positive cells and EGFP-positive, marker-negative cells, respectively.

(D–F) Quantification of sections as in (C) for the percentages of EGFP-positive cells expressing Pax6 (D), Ki67 (E), or Tbr2 (F). *$p < 0.05$, **$p < 0.01$; $n = 3–4$ embryos, 3–5 sections per embryo.

(legend continued on next page)

for Brn1 (Figures 8E, 8G, and 8I). These Brn1-positive, EGFP-positive cells aberrantly expressing deep layer transcription factors were almost all outside of the VZ, with many in the intermediate zone and CP (Figures 8A–8E). These cells were likely neurons because only a small population of EGFP-positive, Ctip2-positive cells outside of the VZ expressed the IP marker Tbr2 (Figure 8J).

We also asked about 4E-T knockdown. Similar electroporations showed that 4E-T knockdown increased the proportion of EGFP-positive, FoxP2 protein-positive cells from approximately 3%–4% to about 15% (Figures 8K and 8L) and that almost all of these FoxP2-positive electroporated cells were also positive for Brn1 (Figures 8K and 8M). Thus, disruption of either Pum2 or 4E-T caused aberrant expression of a deep layer neuron phenotype in a subset of newborn Brn1-positive superficial neurons.

DISCUSSION

During embryogenesis, cortical RPs sequentially generate different neuronal subtypes, with the earliest-born neurons populating deeper cortical layers and later-born neurons more superficial layers. Because it is now clear from lineage-tracing studies that individual RPs generate multiple types of cortical neurons (Guo et al., 2013; Gao et al., 2014; Eckler et al., 2015), a key question involves the molecular mechanisms determining this sequential neurogenesis. Several models could be invoked to explain these findings. In one extensively investigated model, the genes that encode neuronal specification proteins are turned on when a particular neuronal subtype is being generated and then are rapidly turned off when that subtype is no longer made (reviewed in Kwan et al., 2012; Greig et al., 2013). Here we provide evidence for a second, not mutually exclusive model in which RPs are transcriptionally primed to make diverse cortical neuron subtypes and post-transcriptional mechanisms select when and where neuronal specification mRNAs are translated.

The conclusion that RPs are transcriptionally primed to generate diverse cortical neurons comes from the scRNA-seq and FISH analyses. These studies indicate that RPs co-express mRNAs encoding deep and superficial layer specification proteins throughout the neurogenic period. Although there are fewer precursors co-expressing superficial and deep layer mRNAs at E17.5, the end of neurogenesis, there are nonetheless still many RPs and even newborn neurons with this mixed transcriptional phenotype. Precedent for this type of transcriptional priming comes from embryonic stem cells (Efroni et al., 2008) and makes biological sense from several perspectives. First, neurogenesis occurs within a short time frame, and a switch from making one to another neuronal subtype could occur more rapidly if the mRNAs were already present and simply needed to be derepressed. Second, transcriptional priming would allow fast extrinsic regulation of neuronal specification and, thus, provide flexibility within a rapidly changing environment. Third, this model provides a mechanism for rapidly turning protein expression off, as exemplified by our data showing that, in the absence of 4E-T and/or Pum2, deep layer specifiers are aberrantly translated during superficial layer neurogenesis. These studies do not preclude an important role for transcriptional regulation but, instead, provide evidence for an additional regulatory layer that acts to ensure appropriate neuronal specification. These findings are also consistent with previous reports showing that *Fezf2* mRNA persists in the VZ long after deep layer neurons have been generated (Guo et al., 2013), *Cux2* mRNA is expressed in the VZ before superficial layer neurons are made (Nieto et al., 2004; Guo et al., 2013), and Ctip2 protein is only observed in postmitotic subcerebral neurons, whereas *Ctip2* mRNA is expressed in cortical precursors (Leid et al., 2004; Arlotta et al., 2005).

Our findings raise a number of key questions. One of these involves the precise molecular nature of the translational repression complexes. In particular, our work defines a Pum2/4E-T complex that represses mRNAs regulating both the timing and specificity of neurogenesis (this study; Yang et al., 2014). However, many specification mRNAs that are expressed in RPs were not immunoprecipitated with Pum2 and, thus, are likely silenced by other RNA binding proteins and/or microRNAs. Moreover, the Pum2 and 4E-T target mRNAs were only partially overlapping, indicating other protein partners for both of these translational repressors. In this regard, we recently showed that the RNA binding protein Smaug2 interacts with 4E-T in RPs to repress translation of the proneurogenic protein Nanos1 (Amadei et al., 2015).

A second key issue involves the association/dissociation of target mRNAs with Pum2/4E-T complexes. In this regard, both 4E-T and Pum2 are known phosphoproteins, Pumilio proteins are phosphorylated in response to growth factors like EGF (Kedde et al., 2010), and phosphorylation regulates Pumilio activity (Ota et al., 2011). Because embryonic cortical RPs are exposed to many growth factors that regulate neurogenesis (for example, see Yuzwa et al., 2016), then we propose that environmentally driven signaling cascades directly regulate mRNA interactions with Pum2/4E-T complexes. However, simple phosphorylation-based models may not be sufficient to explain selective complex association with target mRNAs. For example, more than half of *Brn1* mRNA, but only 20% of *Tle4* mRNA, is complexed with 4E-T and Pum2 in E12 apical RPs. We believe that this selective association is likely mediated by other, still undefined proteins associating with Pum2, 4E-T, and/or the mRNAs themselves, in agreement with recent data showing that many RNA-binding proteins and components of the translational machinery are expressed and differentially regulated across cortical neurogenesis (DeBoer et al., 2013).

(G) Representative confocal images of electroporated sections immunostained for EGFP (green), Tle4 (red), and Brn1 (turquoise). Boxed regions are shown at higher magnification on the right, with the color channels shown individually. Nuclei are outlined with hatched white ovals, as defined by nuclear EGFP.
(H–J) Quantification of sections as in (G) for the percentage of EGFP-positive cells expressing Brn1 (H), Tle4 (I), or both Brn1 and Tle4 (J) in either the entire cortex (Total Cortex) or in the SVZ, IZ, and CP (Excluding VZ). ***$p < 0.001$, ns = $p > 0.05$; n = 3 embryos each, 3 sections per embryo.
Scale bars, 30 μm in (A) and 10 μm in (C) and (G). Error bars denote SEM. See also Figure S5.

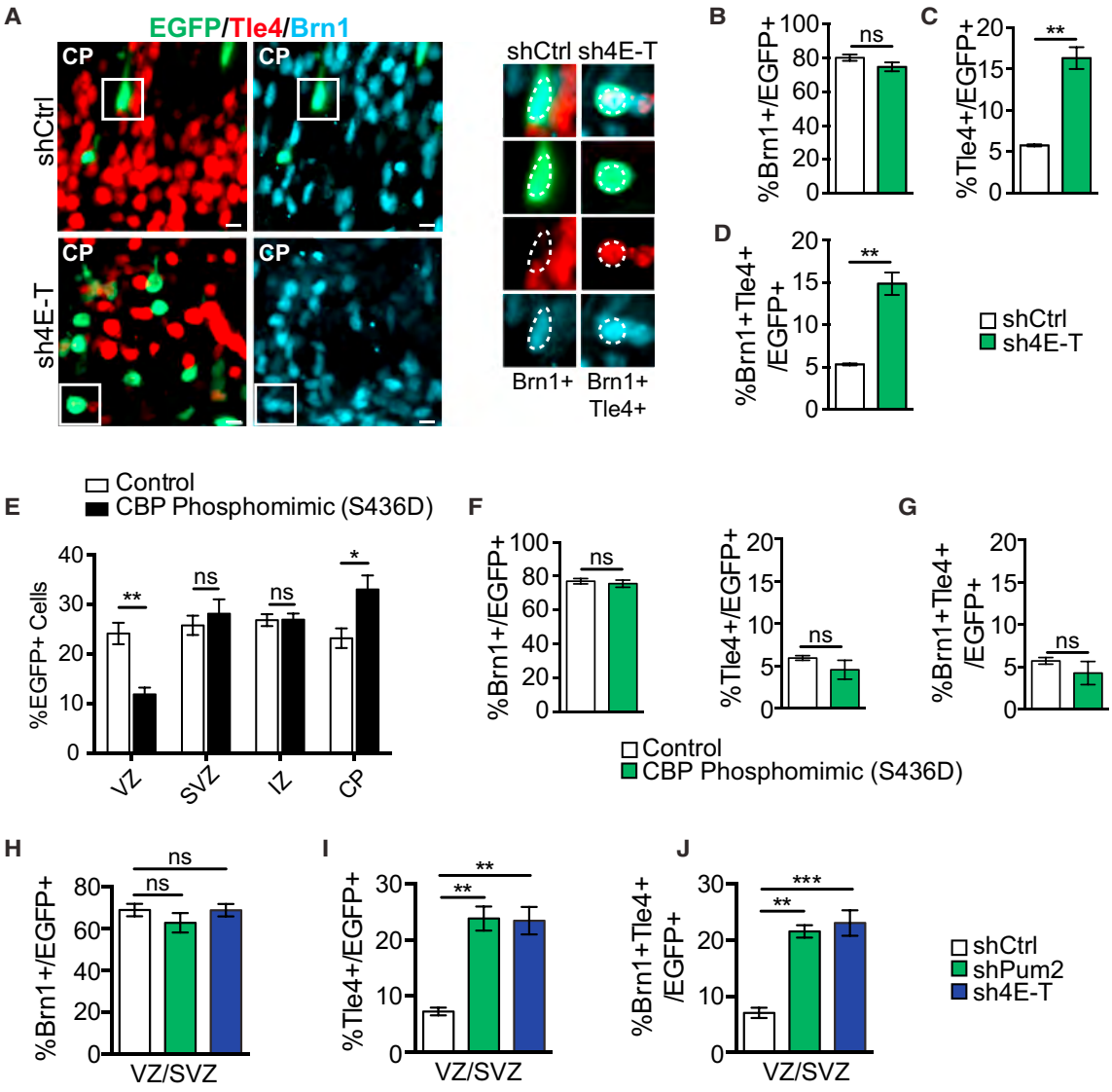

Figure 7. 4E-T Regulates Translation of Brn1 and Tle4 mRNAs during Neurogenesis

(A) E13/E14 cortices were co-electroporated with a nuclear EGFP plasmid and control (shCtrl) or 4E-T (sh4E-T) shRNA, and coronal cortical sections were analyzed 3 days later by immunostaining for EGFP (green), Brn1 (turquoise), and Tle4 (red). Boxed regions are shown at higher magnification on the right, where the different color channels are separated.

(B–D) Quantification of images as in (A) for the percentages of total EGFP-positive cells that were also positive for Brn1 (B), Tle4 (C), or both Brn1 and Tle4 (D). $^{**}p < 0.01$, ns = $p > 0.05$; n = 3 embryos each, 3 sections per embryo.

(E–G) E13/E14 cortices were co-electroporated with a nuclear EGFP plasmid and an expression construct for CBP S436D or the empty vector (control), and coronal cortical sections were immunostained 3 days later for EGFP, Brn1 and Tle4.

(E) Quantification of the percentage of EGFP-positive cells that were in each of the cortical regions. $^{*}p < 0.05$, $^{**}p < 0.01$, ns = $p > 0.05$; n = 3 embryos each, 2–3 sections per embryo.

(F and G) Quantification of the percentages of total EGFP-positive cells that were positive for either Brn1 or Tle4 (F) or for both Brn1 and Tle4 (G). ns ≥ 0.05; n = 3 embryos each, 2–3 sections per embryo.

(H–J) E13/E14 cortices were co-electroporated with a nuclear EGFP plasmid and control (shCtrl), Pum2 (shPum2), or 4E-T (sh4E-T) shRNA, and coronal cortical sections were analyzed 2 days later by immunostaining for EGFP, Brn1, and Tle4 (Figures S6E and S6F). Confocal images of these sections were then quantified for the percentages of total EGFP-positive cells in the VZ/SVZ that were also positive for Brn1 (H), Tle4 (I), or both Brn1 and Tle4 (J). $^{**}p < 0.01$, $^{***}p < 0.001$, ns = $p > 0.05$ by one-way ANOVA with Dunnett's multiple comparisons test; n = 3 embryos each, 2 sections per embryo.

Scale bars, 10 μm. Error bars denote SEM. See also Figure S6.

Our findings raise one final important question. How long does this transcriptional flexibility persist? Our data show that RPs continue to express neuronal specification mRNAs after neurogenesis is complete and that some postnatal neurons express specification mRNAs for diverse neuronal phenotypes when they have already "chosen" a single identity at the protein level.

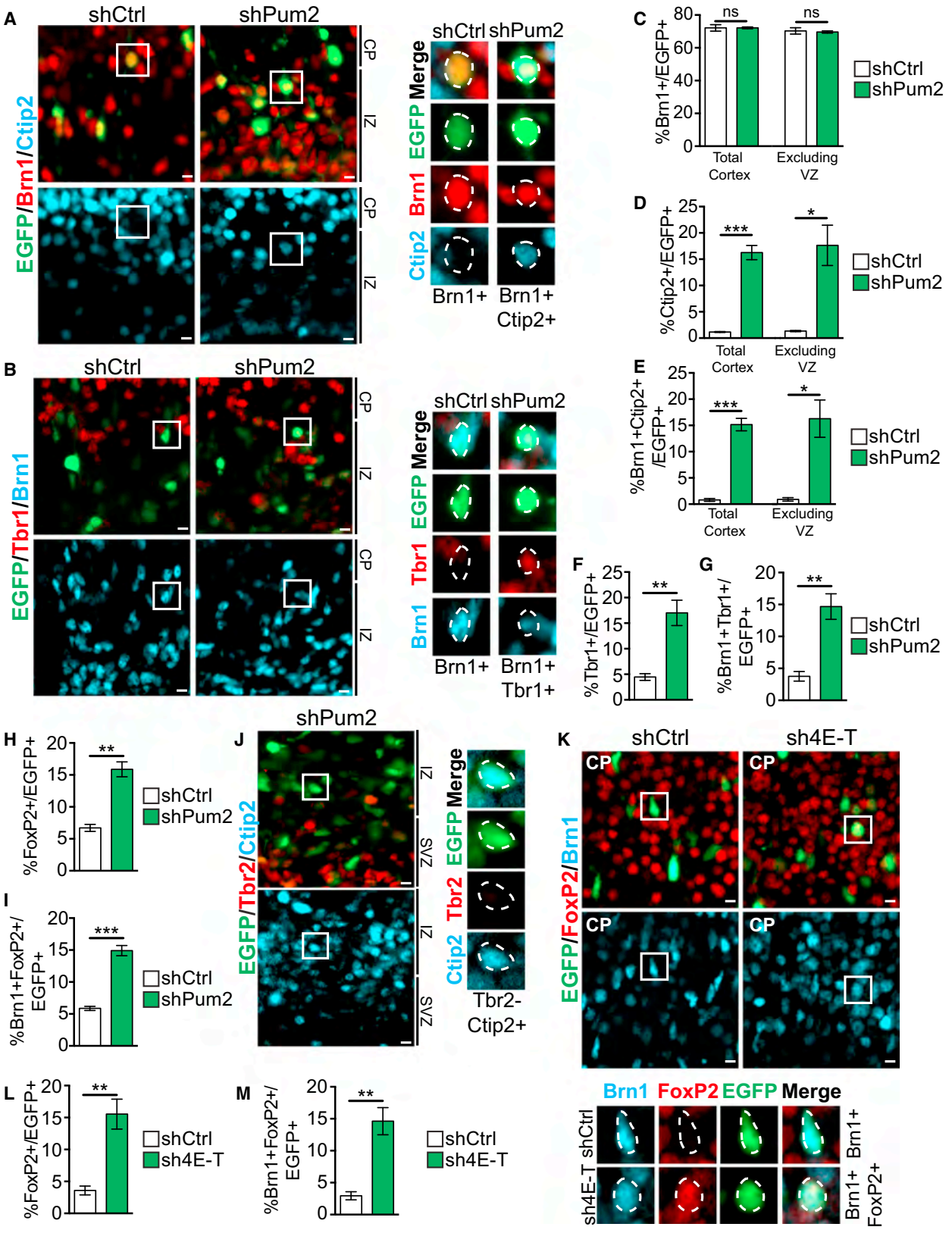

(legend on next page)

These findings may thus reflect a general developmental flexibility with regard to neurogenesis and neuronal phenotypes and may even provide a partial explanation for the ability to reprogram perinatal cortical neurons from one subtype to another with single transcription factors such as Fezf2 (Rouaux and Arlotta, 2013). This type of transcriptional priming may thus reflect a general cellular strategy where post-transcriptional repression mechanisms provide an important way to ensure appropriate differentiation within a rapidly evolving developing environment.

STAR★METHODS

Detailed methods are provided in the online version of this paper and include the following:

- KEY RESOURCES TABLE
- CONTACT FOR REAGENT AND RESOURCE SHARING
- EXPERIMENTAL MODEL AND SUBJECT DETAILS
  - Mice
  - Primary cell cultures and transfections
- METHOD DETAILS
  - Plasmids
  - In utero electroporation
  - Antibodies
  - Immunostaining and histological analysis
  - Protein immunoprecipitation and immunoblotting
  - RNA immunoprecipitation (RIP) and microarray analysis
  - PCR
  - Pum2 motif prediction and knockdown analysis
  - Fluorescence *in situ* hybridization (FISH)
  - Proximity ligation assay (PLA)
  - Single-cell RNA sequencing (scRNAseq)
- QUANTIFICATION AND STATISTICAL ANALYSIS
  - Microscopy and quantification
  - Statistics
- DATA AND SOFTWARE AVAILABILITY

SUPPLEMENTAL INFORMATION

Supplemental Information includes seven figures and five tables and can be found with this article online at https://doi.org/10.1016/j.neuron.2017.12.045.

ACKNOWLEDGMENTS

This work was funded by CIHR grants and the CFREF "Medicine by Design" (to F.D.M. and D.R.K.) and by an EU FP7 Marie Curie grant (to H.K.). F.D.M. is a Canada Research Chair and was an HHMI Senior International Research Scholar during the course of this work. S.K.Z. was funded by a CIHR M.D./Ph.D. studentship, G.Y. by a Brain Canada Mental Health fellowship and an HSC Restracomp/CBMH fellowship, S.A.Y. by OIRM and Lap-Chee Tsui HSC Restracomp postdoctoral fellowships, M.J.B. by an NSERC Masters studentship, and A.V. by CIHR, MSSOC, and HSC Restracomp postdoctoral fellowships. We thank Sarah Burns and Dennis Aquino for technical assistance, Stefano Stifani for the Tle4 antibody, John Vessey for the Pum2 shRNA, and Jing Wang for the CBP phosphomimic expression plasmid.

AUTHOR CONTRIBUTIONS

S.K.Z. conceptualized, designed, performed, and analyzed most of the experiments and co-wrote the paper. G.Y. conceptualized, performed, and analyzed the RIP/microarray experiments and contributed to the qRT-PCR, FISH, culture, and co-immunoprecipitation experiments. H.K. analyzed and validated the RIP experiments. S.A.Y. and M.J.B. performed and analyzed the scRNA-seq experiments, and M.J.B. participated in the FISH analysis. A.V. performed and analyzed the qPCRs. D.R.K. conceptualized experiments and co-wrote the paper. F.D.M. conceptualized and designed experiments, analyzed data, and co-wrote the paper.

DECLARATION OF INTERESTS

The authors declare no competing interests.

Received: August 18, 2017
Revised: November 22, 2017
Accepted: December 28, 2017
Published: January 25, 2018

REFERENCES

Amadei, G., Zander, M.A., Yang, G., Dumelie, J.G., Vessey, J.P., Lipshitz, H.D., Smibert, C.A., Kaplan, D.R., and Miller, F.D. (2015). A Smaug2-based

Figure 8. Pum2 and 4E-T Are Important for Repressing a Deep Layer Neuron Phenotype in Newborn Superficial Layer Neurons

(A–J) E13/E14 cortices were electroporated with a nuclear EGFP plasmid and Pum2 (shPum2) or control (shCtrl) shRNA, and coronal cortical sections were immunostained 3 days later at E16/E17.

(A and B) Representative confocal images of electroporated sections immunostained for EGFP (green, both), Brn1 (red in A; turquoise in B), and either Ctip2 (turquoise; A) or Tbr1 (red; B). Boxed regions are shown at higher magnification on the right, with the color channels shown individually. Nuclei are outlined with hatched white ovals, as defined by nuclear EGFP.

(C–G) Quantification of sections as in (A) and (B) for the percentages of EGFP-positive cells expressing Brn1 (C), Ctip2 (D), Brn1 and Ctip2 (E), Tbr1 (F), or Brn1 and Tbr1 (G) in either the entire cortex (Total Cortex) or in the SVZ, IZ, and CP (Excluding VZ). $^{*}p < 0.05$, $^{**}p < 0.01$, $^{***}p < 0.001$, ns = $p > 0.05$; n = 3 embryos, 3 sections per embryo.

(H and I) Quantification of electroporated sections immunostained for EGFP, Brn1, and FoxP2 (Figure S7) for the percentages of total EGFP-positive cells expressing FoxP2 (H) or Brn1 and FoxP2 (I). $^{**}p < 0.01$, $^{***}p < 0.001$; n = 3 embryos, 3 sections per embryo.

(J) Representative confocal images of an electroporated section immunostained for EGFP (green), Tbr2 (red), and Ctip2 (turquoise). The boxed region is shown at higher magnification on the right, with the color channels shown individually. The nucleus of an EGFP-positive, Ctip2-positive, Tbr2-negative cell is outlined with hatched white ovals, as defined by nuclear EGFP.

(K–M) E13/E14 cortices were electroporated with a nuclear EGFP plasmid and 4E-T (sh4E-T) or control (shCtrl) shRNA, and coronal cortical sections were analyzed 3 days later.

(K) Representative confocal images of sections immunostained for EGFP (green), Brn1 (blue), and FoxP2 (red). Boxed regions are shown at higher magnification at the bottom, with the color channels shown individually. Nuclei are outlined with hatched white ovals, as defined by nuclear EGFP.

(L and M) Quantification of sections as in (K) for the percentages of total EGFP-positive cells expressing FoxP2 (L) or Brn1 and FoxP2 (M). $^{**}p < 0.01$; n = 3 embryos, 3 sections per embryo.

Scale bars, 10 μm. Error bars denote SEM. See also Figure S7.

translational repression complex determines the balance between precursor maintenance versus differentiation during mammalian neurogenesis. J. Neurosci. *35*, 15666–15681.

Arlotta, P., Molyneaux, B.J., Chen, J., Inoue, J., Kominami, R., and Macklis, J.D. (2005). Neuronal subtype-specific genes that control corticospinal motor neuron development in vivo. Neuron *45*, 207–221.

Barnabé-Heider, F., Wasylnka, J.A., Fernandes, K.J.L., Porsche, C., Sendtner, M., Kaplan, D.R., and Miller, F.D. (2005). Evidence that embryonic neurons regulate the onset of cortical gliogenesis via cardiotrophin-1. Neuron *48*, 253–265.

Bolte, S., and Cordelières, F.P. (2006). A guided tour into subcellular colocalization analysis in light microscopy. J. Microsc. *224*, 213–232.

Costes, S.V., Daelemans, D., Cho, E.H., Dobbin, Z., Pavlakis, G., and Lockett, S. (2004). Automatic and quantitative measurement of protein-protein colocalization in live cells. Biophys. J. *86*, 3993–4003.

DeBoer, E.M., Kraushar, M.L., Hart, R.P., and Rasin, M.R. (2013). Post-transcriptional regulatory elements and spatiotemporal specification of neocortical stem cells and projection neurons. Neuroscience *248*, 499–528.

Dominguez, M.H., Ayoub, A.E., and Rakic, P. (2013). POU-III transcription factors (Brn1, Brn2, and Oct6) influence neurogenesis, molecular identity, and migratory destination of upper-layer cells of the cerebral cortex. Cereb. Cortex *23*, 2632–2643.

Eckler, M.J., Nguyen, T.D., McKenna, W.L., Fastow, B.L., Guo, C., Rubenstein, J.L.R., and Chen, B. (2015). Cux2-positive radial glial cells generate diverse subtypes of neocortical projection neurons and macroglia. Neuron *86*, 1100–1108.

Efroni, S., Duttagupta, R., Cheng, J., Dehghani, H., Hoeppner, D.J., Dash, C., Bazett-Jones, D.P., Le Grice, S., McKay, R.D.G., Buetow, K.H., et al. (2008). Global transcription in pluripotent embryonic stem cells. Cell Stem Cell *2*, 437–447.

Gallagher, D., Voronova, A., Zander, M.A., Cancino, G.I., Bramall, A., Krause, M.P., Abad, C., Tekin, M., Neilsen, P.M., Callen, D.F., et al. (2015). Ankrd11 is a chromatin regulator involved in autism that is essential for neural development. Dev. Cell *32*, 31–42.

Gao, P., Postiglione, M.P., Krieger, T.G., Hernandez, L., Wang, C., Han, Z., Streicher, C., Papusheva, E., Insolera, R., Chugh, K., et al. (2014). Deterministic progenitor behavior and unitary production of neurons in the neocortex. Cell *159*, 775–788.

Gauthier, A.S., Furstoss, O., Araki, T., Chan, R., Neel, B.G., Kaplan, D.R., and Miller, F.D. (2007). Control of CNS cell-fate decisions by SHP-2 and its dysregulation in Noonan syndrome. Neuron *54*, 245–262.

Greig, L.C., Woodworth, M.B., Galazo, M.J., Padmanabhan, H., and Macklis, J.D. (2013). Molecular logic of neocortical projection neuron specification, development and diversity. Nat. Rev. Neurosci. *14*, 755–769.

Guo, C., Eckler, M.J., McKenna, W.L., McKinsey, G.L., Rubenstein, J.L.R., and Chen, B. (2013). Fezf2 expression identifies a multipotent progenitor for neocortical projection neurons, astrocytes, and oligodendrocytes. Neuron *80*, 1167–1174.

Huang, W., Sherman, B.T., and Lempicki, R.A. (2009). Systematic and integrative analysis of large gene lists using DAVID bioinformatics resources. Nat. Protoc. *4*, 44–57.

Kedde, M., van Kouwenhove, M., Zwart, W., Oude Vrielink, J.A.F., Elkon, R., and Agami, R. (2010). A Pumilio-induced RNA structure switch in p27-3′ UTR controls miR-221 and miR-222 accessibility. Nat. Cell Biol. *12*, 1014–1020.

Kwan, K.Y., Sestan, N., and Anton, E.S. (2012). Transcriptional co-regulation of neuronal migration and laminar identity in the neocortex. Development *139*, 1535–1546.

Leid, M., Ishmael, J.E., Avram, D., Shepherd, D., Fraulob, V., and Dollé, P. (2004). CTIP1 and CTIP2 are differentially expressed during mouse embryogenesis. Gene Expr. Patterns *4*, 733–739.

Mi, H., Muruganujan, A., Casagrande, J.T., and Thomas, P.D. (2013). Large-scale gene function analysis with the PANTHER classification system. Nat. Protoc. *8*, 1551–1566.

Miller, M.A., and Olivas, W.M. (2011). Roles of Puf proteins in mRNA degradation and translation. Wiley Interdiscip. Rev. RNA *2*, 471–492.

Nieto, M., Monuki, E.S., Tang, H., Imitola, J., Haubst, N., Khoury, S.J., Cunningham, J., Gotz, M., and Walsh, C.A. (2004). Expression of Cux-1 and Cux-2 in the subventricular zone and upper layers II-IV of the cerebral cortex. J. Comp. Neurol. *479*, 168–180.

Ota, R., Kotani, T., and Yamashita, M. (2011). Possible involvement of Nemo-like kinase 1 in Xenopus oocyte maturation as a kinase responsible for Pumilio1, Pumilio2, and CPEB phosphorylation. Biochemistry *50*, 5648–5659.

Quenault, T., Lithgow, T., and Traven, A. (2011). PUF proteins: repression, activation and mRNA localization. Trends Cell Biol. *21*, 104–112.

Ray, D., Kazan, H., Chan, E.T., Peña Castillo, L., Chaudhry, S., Talukder, S., Blencowe, B.J., Morris, Q., and Hughes, T.R. (2009). Rapid and systematic analysis of the RNA recognition specificities of RNA-binding proteins. Nat. Biotechnol. *27*, 667–670.

Ritchie, M.E., Phipson, B., Wu, D., Hu, Y., Law, C.W., Shi, W., and Smyth, G.K. (2015). limma powers differential expression analyses for RNA-sequencing and microarray studies. Nucleic Acids Res. *43*, e47.

Rouaux, C., and Arlotta, P. (2013). Direct lineage reprogramming of post-mitotic callosal neurons into corticofugal neurons in vivo. Nat. Cell Biol. *15*, 214–221.

Shen, Q., Wang, Y., Dimos, J.T., Fasano, C.A., Phoenix, T.N., Lemischka, I.R., Ivanova, N.B., Stifani, S., Morrisey, E.E., and Temple, S. (2006). The timing of cortical neurogenesis is encoded within lineages of individual progenitor cells. Nat. Neurosci. *9*, 743–751.

Sugitani, Y., Nakai, S., Minowa, O., Nishi, M., Jishage, K., Kawano, H., Mori, K., Ogawa, M., and Noda, T. (2002). Brn-1 and Brn-2 share crucial roles in the production and positioning of mouse neocortical neurons. Genes Dev. *16*, 1760–1765.

Tsui, D., Vessey, J.P., Tomita, H., Kaplan, D.R., and Miller, F.D. (2013). FoxP2 regulates neurogenesis during embryonic cortical development. J. Neurosci. *33*, 244–258.

Vessey, J.P., Vaccani, A., Xie, Y., Dahm, R., Karra, D., Kiebler, M.A., and Macchi, P. (2006). Dendritic localization of the translational repressor Pumilio 2 and its contribution to dendritic stress granules. J. Neurosci. *26*, 6496–6508.

Vessey, J.P., Schoderboeck, L., Gingl, E., Luzi, E., Riefler, J., Di Leva, F., Karra, D., Thomas, S., Kiebler, M.A., and Macchi, P. (2010). Mammalian Pumilio 2 regulates dendrite morphogenesis and synaptic function. Proc. Natl. Acad. Sci. USA *107*, 3222–3227.

Vessey, J.P., Amadei, G., Burns, S.E., Kiebler, M.A., Kaplan, D.R., and Miller, F.D. (2012). An asymmetrically localized Staufen2-dependent RNA complex regulates maintenance of mammalian neural stem cells. Cell Stem Cell *11*, 517–528.

Wang, J., Weaver, I.C.G., Gauthier-Fisher, A., Wang, H., He, L., Yeomans, J., Wondisford, F., Kaplan, D.R., and Miller, F.D. (2010). CBP histone acetyltransferase activity regulates embryonic neural differentiation in the normal and Rubinstein-Taybi syndrome brain. Dev. Cell *18*, 114–125.

Wang, J., Gallagher, D., DeVito, L.M., Cancino, G.I., Tsui, D., He, L., Keller, G.M., Frankland, P.W., Kaplan, D.R., and Miller, F.D. (2012). Metformin activates an atypical PKC-CBP pathway to promote neurogenesis and enhance spatial memory formation. Cell Stem Cell *11*, 23–35.

Wickens, M., Bernstein, D.S., Kimble, J., and Parker, R. (2002). A PUF family portrait: 3'UTR regulation as a way of life. Trends Genet. *18*, 150–157.

Yang, G., Smibert, C.A., Kaplan, D.R., and Miller, F.D. (2014). An eIF4E1/4E-T complex determines the genesis of neurons from precursors by translationally repressing a proneurogenic transcription program. Neuron *84*, 723–739.

Yao, J., Liu, Y., Husain, J., Lo, R., Palaparti, A., Henderson, J., and Stifani, S. (1998). Combinatorial expression patterns of individual TLE proteins during cell determination and differentiation suggest non-redundant functions for mammalian homologs of Drosophila Groucho. Dev. Growth Differ. *40*, 133–146.

Yuzwa, S.A., Yang, G., Borrett, M.J., Clarke, G., Cancino, G.I., Zahr, S.K., Zandstra, P.W., Kaplan, D.R., and Miller, F.D. (2016). Proneurogenic ligands defined by modeling developing cortex growth factor communication networks. Neuron *91*, 988–1004.

Yuzwa, S.A., Borrett, M.J., Innes, B.T., Voronova, A., Ketela, T., Kaplan, D.R., Bader, G.D., and Miller, F.D. (2017). Developmental emergence of adult neural stem cells as revealed by single-cell transcriptional profiling. Cell Rep. *21*, 3970–3986.

STAR★METHODS

KEY RESOURCES TABLE

REAGENT or RESOURCE	SOURCE	IDENTIFIER
Antibodies		
mouse anti-4E-T	Novus Biologicals	Cat# H00056478-B01P; RRID: AB_1673784
chicken anti-eGFP	Abcam	Cat# ab13970; RRID: AB_300798
rabbit anti-βIII-tubulin	Biolegend	Cat# 802001; clone# Poly18020; RRID: AB_2564645
mouse anti-βIII-tubulin	Biolegend	Cat# 801202; clone# TUJ1; RRID: AB_10063408
mouse anti-Ki67	BD PharMingen	Cat# 556003; RRID: AB_396287
rabbit anti-Pax6	Biolegend	Cat# 901301; RRID: AB_2565003
rabbit anti-Tbr2	Abcam	Cat# ab23345; RRID: AB_778267
rat anti-Ctip2	Abcam	Cat# ab18465; RRID: AB_2064130
rabbit anti-Tle4	Laboratory of Stefano Stifani; Yao et al., 1998	N/A
rabbit anti-Pumilio2	MBL	Cat# RN027P; RRID: AB_1953053
rabbit anti-Pumilio2	Bethyl Laboratories	Cat# A300-202A;RRID: AB_2173752
goat anti-Brn1/2	Santa Cruz Biotechnology	Cat# sc-6029; RRID:AB_2167385
goat anti-Brn1	Novus Biologicals	Cat# NBP1-49872; RRID: AB_10012062
mouse anti-NPY-R (E-4)	Santa Cruz Biotechnology	Cat# sc-393192; RRID: AB_2721049
rabbit anti-FoxP2	Abcam	Cat# ab16046; RRID: AB_2107107
rabbit anti-Tbr1	Abcam	Cat# ab31940; RRID:AB_2200219
mouse anti-Dcp1	Novus Biologicals	Cat# H00055802-M06; RRID: AB_538184
rabbit anti-Cleaved Caspase 3	Cell Signaling	Cat# 9661; RRID: AB_2341188
normal mouse IgG	Millipore	Cat# 12-371; RRID: AB_145840
normal rabbit IgG	Milipore	Cat # 12-370; RRID:AB_145841
Bacterial and Virus Strains		
NEB 5-alpha Competent E.coli (High Efficiency)	NEB	Cat# C2987H
Biological Samples		
Embryonic and postnatal cortices and brains from CD1 mice described in Experimental Models: Organisms/Strains below.	This paper	N/A
Critical Commercial Assays		
RNAscope Fluorescent Multiplex Detection Reagents	ACDBio	Cat# 320851
Magna RIP RNA-Binding Protein Immunoprecipitation Kit	Millipore	Cat# 17-700
GeneChip Pico Kit	Thermo Fisher	Cat# 902622
DuoLink *in situ* Red Starter Kit Mouse/Rabbit	Sigma-Aldrich	Cat# DUO92101
Deposited Data		
Single cell RNA sequencing data from E13.5, E15.5, and E17.5 murine cortex	Yuzwa et al., 2017	GEO: GSE107122
Raw and analyzed microarray data from 4E-T RIP	Yang et al., 2014	GEO: GSE61729
Raw and analyzed microarray data from Pum2 RIP	This paper	GEO: GSE108404
Experimental Models: Organisms/Strains		
CD1	Charles River	Cat #022

(*Continued on next page*)

Continued

REAGENT or RESOURCE	SOURCE	IDENTIFIER
Oligonucleotides		
For Pum2 shRNA sequence, please see Table S1	Vessey et al., 2006	N/A
For 4E-T shRNA sequence, please see STAR Methods	Yang et al., 2014	N/A
For CBP S436D sequence, please see STAR Methods	Wang et al., 2010	N/A
For qPCR primer sequences, please see Table S5	This paper	N/A
Recombinant DNA		
pSUPER vector	Oligoengine	Cat# VEC-PBS-0002
pEF-GFP	Barnabé-Heider et al., 2005	N/A
pcDNA3.1(-)	Thermo-Fisher	Cat# V79520
Software and Algorithms		
GraphPad Prism 6	GraphPad Software	https://www.graphpad.com/scientific-software/prism/; RRID: SCR_002798
Volocity software (version 6.3)	Perkin Elmer	http://www.perkinelmer.com/pages/020/cellularimaging/products/volocity.xhtml; RRID: SCR_002668
ZEN software (version 2.3)	ZEISS	https://www.zeiss.com/microscopy/int/products/microscope-software/zen.html; RRID: SCR_013672
Adobe Illustrator CS6	Adobe	http://www.adobe.com/products/illustrator.html; RRID: SCR_010279
Adobe Photoshop CS6	Adobe	https://www.adobe.com/products/photoshop.html; RRID: SCR_014199
ImageJ "Just Another Colocalization Plugin" (version 1)	NIH	https://imagej.nih.gov/ij/; RRID: SCR_003070
limma R package (version 3.30.13)	Ritchie et al., 2015	http://bioinf.wehi.edu.au/limma/; RRID:SCR_010943
Affymetrix Expression Console Software	Thermo Fisher Scientific	http://www.affymetrix.com; RRID:SCR_010231
DAVID Gene Ontology Analysis (version 6.8)	Huang et al., 2009	http://david.abcc.ncifcrf.gov/; RRID:SCR_001881
PANTHER Classification System (version 13.0)	Mi et al., 2013	http://www.pantherdb.org/; RRID:SCR_004869
RNAcompete	Ray et al., 2009	https://doi.org/10.1038/nbt.1550; RRID:SCR_015900
Ensembl BioMart	European Bioinformatics Institute	http://www.ensembl.org/biomart; RRID:SCR_002344
Seurat R package (version 1.4)	Laboratory of Rahul Satija	http://satijalab.org/seurat/
Other		
FISH probe: Mouse *Brn1* (GenBank: NM_008900), channel 1	ACDBio	Cat #441521
FISH probe: Mouse *Tle4* (GenBank: NM_011600), channel 2	ACDBio	Cat #417301-C2
FISH probe: Mouse *Tle3* (GenBank: NM_001083927.1), channel 1	ACDBio	Cat #448501
FISH probe: Mouse *Diap3* (GenBank: NM_019670.1), channel 3	ACDBio	Cat #441511-C3
FISH probe: Mouse *Glo1* (GenBank: NM_025374.3), channel 2	ACDBio	Cat #417311-C2
FISH probe: Mouse *Vcam1* (GenBank: NM_011693.3), channel 1	ACDBio	Cat #438641
FISH probe: Mouse *Aldoc* (GenBank: NM_009657.3), channel 3	ACDBio	Cat #429531-C3
FISH probe: Mouse *Ctip2* (GenBank: NM_021399.2), channel 1	ACDBio	Cat #413271

CONTACT FOR REAGENT AND RESOURCE SHARING

Further information and requests for resources and reagents should be directed to and will be fulfilled by the Lead Contact, Freda Miller (fredam@sickkids.ca).

EXPERIMENTAL MODEL AND SUBJECT DETAILS

Mice

All animal use was approved by the Animal Care Committee of the Hospital for Sick Children in accordance with the Canadian Council of Animal Care policies. Mice were maintained on a 12hr light/dark cycle, and food and water was provided *ad libitum*. All mice were healthy with no obvious behavioral phenotypes, and none of the experimental mice were immune compromised. For all studies, mice of either sex were used and mice were randomly allocated to experimental groups. Embryonic (E) day 11-17 and postnatal (P) day 3 mice were used. Wild-type CD1 mice (Charles River Laboratories) were used for all culture and electroporation experiments.

Primary cell cultures and transfections

Primary cell cultures were prepared as previously described (Yang et al., 2014). Briefly, cortices were dissected from pooled E11-E13 CD1 mouse embryos of either sex from the same mother. The meninges were removed and the exposed cortex was collected and mechanically triturated. Dissociated cortical precursor cells were cultured at 37°C in Neurobasal medium (Invitrogen) supplemented with 2% B27 (Invitrogen), 0.5 mM L-glutamine (Invitrogen) and 40 ng/ml FGF2 (BD Biosciences), at a density of 300,000 cells/ml on glass coverslips precoated with 2% laminin (BD Biosciences) and 1% poly-D-lysine (Sigma), and transfected with Lipofectamine LTX (Invitrogen) according to the manufacturer's instructions. For co-transfection, a 1:3 ratio of EGFP to shRNA (total 1 μg/well) was used. Cells were collected and immunostained 48hr or 72hrs later.

METHOD DETAILS

For all experiments, mouse embryos were randomly allocated to experimental groups and all data collected throughout these studies were included in the analyses. No data were excluded (no exclusion criteria). No sample-size estimates were conducted due to technical limitations on sample collection. All attempts were made to use a maximal sample size in each experiment whenever possible

Plasmids

The pEF-EGFP plasmid expressing nuclear EGFP (Barnabé-Heider et al., 2005), the pcDNA3.1(-) plasmid expressing the CBP phosphomimic (Wang et al., 2010, 2012), and the shRNAs against 4E-T (Yang et al., 2014) or Pumilio2 (Vessey et al., 2012) have been previously described.

In utero electroporation

CD1 timed pregnant mice were used for in utero electroporations as previously described (Gauthier et al., 2007). Briefly, an expression construct for nuclear EGFP was coelectroporated with shRNA constructs at a 1:3 ratio. Prior to injection, plasmids were mixed with 0.5% trypan blue. Following injection into the lateral ventricles, the square electroporator CUY21 EDIT (TR Tech, Japan) was used to deliver five 50 ms pulses of 40-50 V with 950 ms intervals per embryo. Brains were dissected 48hr or 72hrs later and analyzed post electroporation at indicated developmental stages.

Antibodies

The primary antibodies used were mouse anti-4E-T (Novus Biologicals, 1:500), chicken anti-GFP (Abcam, 1:2000, RRID: AB_300798), mouse anti-Ki67 (BD Biosciences PharMingen, 1:500, RRID: AB_396287), mouse anti-βIII-tubulin (Biolegend, 1:1000, RRID: AB_10063408), rabbit anti-βIII-tubulin (Biolegend, 1:1000, RRID: AB_2564645), rabbit anti-Pax6 (Biolegend, 1:2000, RRID: AB_2565003), rabbit anti-Tbr2 (Abcam, 1:500, RRID: AB_778267), rat anti-Ctip2 (Abcam, 1:200, RRID: AB_2064130), rabbit anti-Tle4 (gift from Stefano Stifani, 1:500), rabbit anti-Pumilio2 (MBL, 1:1000, RRID: AB_1953053), rabbit anti-Pumilio2 (Bethyl Laboratories, 1:500, RRID: AB_2173752), goat anti-Brn1/2 (Santa Cruz Biotechnology, 1:250, RRID: AB_2167385), goat anti-Brn1 (Novus Biologicals, 1:400, RRID: AB_10012062), mouse anti-NPY-R (E-4) (Santa Cruz Biotechnology, 1:1000, RRID: AB_2721049), rabbit anti-FoxP2 (Abcam, 1:8000, RRID: AB_2107107), rabbit anti-Tbr1 (Abcam, 1:1000, RRID: AB_2200219), mouse anti-Dcp1 (Novus Biologicals, 1:1000, RRID: AB_538184), and rabbit anti-Cleaved Caspase 3 (Cell Signaling, 1:500, RRID: AB_2341188). The Alexa350, Alexa488, Alexa555, and Alexa647-conjugated secondary antibodies were obtained from Invitrogen. HRP-conjugated goat anti-mouse or anti-rabbit secondary antibodies were purchased from Boehringer Mannheim.

Immunostaining and histological analysis

Immunocytochemistry on cultured cells was performed as previously described (Yang et al., 2014). Briefly, cells on glass coverslips were fixed for 15 minutes with 4% buffered paraformaldehyde (PFA), followed by 3 washes with PBS and permeabilization with 0.3% Triton X-100 diluted in PBS for 3 minutes. Cells were subsequently blocked with 2% bovine serum albumin (BSA) (Jackson ImmunoResearch Laboratories) in PBS and incubated with primary antibodies in PBS overnight at 4°C. Samples were washed 3 times with PBS, and secondary antibodies, diluted in PBS (1:1000), were added for an additional hour at room temperature. Nuclei were counterstained with Hoechst 33258 (Sigma). Coverslips were mounted on glass slides. For immunostaining of cortical sections, embryonic brains were dissected in ice-cold HBSS, fixed in 4% paraformaldehyde at 4°C overnight, cryopreserved with 30% sucrose overnight, and placed in OCT at −80°C for at least a few hours. Brains were cryosectioned coronally at 16 μm. Sections were blocked

at room temperature with 5% BSA and 0.3% Triton X-100 in PBS, and incubated with primary antibodies in 1/2 blocking buffer overnight at 4°C. Sections were washed 3 times with PBS and incubated with appropriate secondary antibodies in PBS at room temperature for 1 hour. Sections were counterstained with Hoechst 33258 (Sigma) and mounted as described above.

Protein immunoprecipitation and immunoblotting

Freshly dissected cerebral cortices from E12-13 mouse embryos were lysed with Gentle Lysis Buffer (GLB) containing 25 mM Tris-HCl (pH 7.4), 2 mM EDTA, 1 mM EGTA, 10 mM NaCl, 0.5% Triton X-100 and 10% glycerol supplemented with the Complete Protease Inhibitor Tablets (Roche Applied Science) and 1mM PMSF. Lysates were precleared by incubating with Protein A/G magnetic beads (Millipore) for 30 min at 4°C, followed by incubation with 5 μg mouse anti-4E-T antibody (Novus Biologicals), or normal mouse IgG (Millipore, RRID: AB_145840) at 4°C for 2 hours, followed by a 1 hour incubation with protein A/G magnetic beads at 4°C. Immunoprecipitates were washed three times with GLB buffer, boiled in 2x sample buffer with 1mM dithiothreitol (DTT) for 3 minutes, and analyzed with SDS-PAGE as described previously (Amadei et al., 2015).

RNA immunoprecipitation (RIP) and microarray analysis

E12-13 cortical lysates used for immunoprecipitations were analyzed using the Magna RIP RNA-Binding Protein Immunoprecipitation Kit in RNase-free conditions on ice, following the manufacturer's instructions (Millipore). Briefly, input lysates were precleared with protein A/G beads and incubated with 5 μg rabbit anti-Pumilio2 antibody (MBL) or normal rabbit IgG (Millipore, RRID: AB_145841) for 3 hours at 4°C. Total RNA was isolated from the input lysates and from the immunoprecipitations, extracted with phenol/chloroform, and the quality of RNA was checked on a BioAnalyzer (Agilent). RNA samples from three biological replicates each of total embryonic cortical input lysates, IgG control immunoprecipitates and Pum2 immunoprecipitates were amplified using the GeneChip Pico Kit (Thermo Fisher) and subjected to microarray analysis using Mouse Gene 2.0 ST Arrays (Thermo Fisher). The raw data obtained from the microarrays was normalized using robust multiarray analysis in the Expression Console (Thermo Fisher) program. After filtering out probesets for non-protein-coding genes, the *limma* package in R (Ritchie et al., 2015) was used to calculate log fold changes for IgG RIP over the input, and transcripts with log fold change (LFC) > 0.58 (FC > 1.5) were removed. The log fold changes for Pum2 RIP over input were then calculated. The Pum2 targets were defined as transcripts with LFC > 0.58 (FC > 1.5) and adjusted p values < 0.05. Similarly, the Pum2 background set included transcripts with LFCs < 0 (FC < 1) and adjusted p values < 0.05. The enriched probe sets were analyzed using DAVID (Huang et al., 2009) and the PANTHER Classification System (Mi et al., 2013).

PCR

cDNA generated from GeneChip Pico Kit (see RNA immunoprecipitation (RIP) and microarray analysis) was used for PCR. PCR was done with amplification for 35 cycles with annealing temperature at approximately 60°C for all primers, using Phusion High-Fidelity DNA Polymerase (NEB). For quantitative real-time PCR, 10 μL PCR reaction mixture containing FastStart DNA Master SYBR Green I (Roche Molecular Biochemicals) was prepared according to the manufacturer's instruction, and loaded on to a 96 multiwell plate. The LightCycler 480 thermocycler (Roche Molecular Biochemicals) was used with a protocol involving an initial activation cycle (2 min, 95°C), 45 cycles of denaturation (10 s, 95°C), annealing (20 s, 60°C) and elongation (20 s, 72°C). A single fluorescence reading was acquired at the end of each elongation step. A melting curve analysis cycle was performed after the PCR amplification. The primers used in RT-qPCR were: *Celsr2* forward 5′-CAC GAT GGC CTG AGG GTT T-3′ and reverse 5′-CCT TGT GGA GAA AGG TGT CCT-3′; *Cox6b1* forward 5′-ACT ACC TGG ACT TCC ACC G-3′ and reverse 5′-ACC CAT GAC ACG GGA CAG A-3′; *4E-T* forward 5′-GAC TGC ATT CAA CAA GCT AGT GA-3′ and reverse 5′-GGG GCC AAT AAG TGA CTT TCA AC-3′; *Foxf2* forward 5′-CGT CCT CTT CTA ACT CCG TCA-3′ and reverse 3′-ATG TAC GAG TAA GGA GGC TTC T-3′; *Foxq1* forward 5′-AAA TTG GAG GTG TTC GTC CCA-3′ and reverse 5′-TCC CCG TCT GAG CCT AAG G-3′; *Mmd2* forward 5′-AGT ATG AAC ACG CAG CAA ACT-3′ and reverse 5′-TCC CAG TCG TCA TCG GAC A-3′; *Neurog1* forward 5′-CCA GCG ACA CTG AGT CCT G-3′ and reverse 5′-CGG GCC ATA GGT GAA GTC TT-3′; *Neurog2* forward 5′-AAC TCC ACG TCC CCA TAC AG-3′ and reverse 5′-GAG GCG CAT AAC GAT GCT TC-3′; *Neurod1* forward 5′-ATG ACC AAA TCA TAC AGC GAG AG-3′ and reverse 5′-TCT GCC TCG TGT TCC TCG T-3′; *Brn1* forward 5′-AGCA GTTCGCTAAGCAGTTCA-3′ and reverse 5′-CGA AGC GGC AGA TAG TGG TC-3′; *Brn4* forward 5′- CTG CCT CGA ATC CCT ACA GC-3′ and reverse 5′-CTG CAA GTA GTC ACT TTG GAG AA-3′; *Prox1* forward 5′-AGA AGG GTT GAC ATT GGA GTG A-3′ and reverse 5′-TGC GTG TTG CAC CAC AGA ATA-3′; *Ptpru* forward 5′-GCT CAG TAT GAC GAC TTC CAA TG-3′ and reverse 5′-TTG ACC ATC AAG TAG GCA CCA-3′; *Rabgef1* forward 5′-ATG AGC CTG AAG TCC GAA CG-3′ and reverse 5′-GCC TTG TGG TAC TCC TCC CT-3′; *Sepp1* forward 5′-AGC TCT GCT TGT TAC AAA GCC-3′ and reverse 5′-CAG GTC TTC CAA TCT GGA TGC-3′; *Tle3* forward 5′-GAG ACT GAA CAC AAT CCT AGC C-3′ and reverse 5′-GGA GTC CAC GTA CCC CGA T-3′; *Tle4* forward 5′-CTG GAC AGG TGG TTT GGA CAA-3′ and reverse 5′-GAG GTG AAG TCA TGT TGC TGC-3′; *Tspan14* forward 5′-GGC TGG CTG GAG TTG TCT TC-3′ and reverse 5′-GGT CGA TTC CAT GCA ACC G-3′.

Pum2 motif prediction and knockdown analysis

For motif prediction, the top 10 n-mers from the position frequency matrix (PFM) inferred by RNAcompete for PUM were generated (Ray et al., 2009) and used to count the number of occurrences of motifs in 3′UTRs of mRNAs from 4ET-RIP target and background sets. To determine how well these motif counts could distinguish between the mRNAs in the target and background sets, we used the

area under the ROC curve (AUROC) metric that measures the expected proportion of positives ranked before a randomly drawn negative example. To this end, the mRNAs in the 4ET-RIP target and background sets were labeled with 1 and 0, respectively. The counts for motif occurrences were used as a prediction score. Pum1/2 had an AU-ROC of ~0.79.

Ortholog genes between mouse and human were retrieved from Ensembl through BioMart (http://www.ensembl.org/biomart on November 1, 2016).

Fluorescence *in situ* hybridization (FISH)

The single molecule FISH was performed with probes targeting *Brn1* (NM_008900), *Tle4* (NM_011600), *Tle3* (NM_001083927.1), *Diap3* (NM_019670.1), *Glo1* (NM_025374.3), *Vcam1* (NM_011693.3), *Aldoc* (NM_009657.3) and *Ctip2* (NM_021399.2) using the RNAscope kit (Advanced Cell Diagnostics), according to the manufacturer's instructions. Briefly, freshly dissected embryonic brains were fixed overnight with RNase-free 4% PFA, cryopreserved overnight with RNase-free 30% sucrose, and placed in OCT at −80°C overnight. Brains were cryosectioned coronally at 16 μm. Sections were washed with ethanol, followed by tissue pretreatment, probe hybridization, and signal amplification. Alternatively, cortical precursor cultures from E12-13 cortices were maintained for 3 days before fixation, ethanol wash, probe hybridization, and signal amplification. In both cases, positive staining was identified as punctate dots present in the nucleus and/or cytoplasm. For simultaneous immunodetection of a particular protein after FISH, sections or cultures were blocked and incubated with the relevant primary antibody overnight at 4°C, followed by 1 hour incubation with the appropriate Alexa-conjugated secondary antibody at room temperature before DAPI staining. Z stacks of confocal images were taken with optical slice thickness of 0.1 μm. The VZ/SVZ region of 40X confocal images were divided into 5 bins of identical area; the total number of mRNA granules in each bin (~100-200 mRNA granules/bin and ~500-1000 mRNA granules/section) were used for quantification of colocalization. Bright and clear mRNA granules that overlapped with immunostained 4E-T or Pum2 were counted using Volocity software (Perkin Elmer). About 160 Z stacked images encompassing each bin were used for this analysis.

Proximity ligation assay (PLA)

PLA was performed as described previously (Amadei et al., 2015) with a DuoLink *in situ* Red Starter Kit Mouse/Rabbit (Sigma) according to the manufacturer's instructions. Briefly, coverslips were incubated with the appropriate primary antibodies, followed by incubation with the secondary antibodies provided in the kit for 1 hour, followed by ligation reaction for 30 minutes, and signal amplification reaction for 1 hour and 40 minutes. All incubation steps were performed at 37°C in a humidified chamber. Following signal amplification and wash steps, the coverslips were mounted with the DAPI-containing mounting medium provided in the kit.

Single-cell RNA sequencing (scRNAseq)

scRNAseq data collected from the embryonic cortex, using the Drop-seq method, is described in Yuzwa et al. (2017) (GEO: GSE107122) and was analyzed using the same computational pipeline. scRNAseq data from embryonic ages E13.5, E15.5, and E17.5 was visualized by t-SNE projections with the overlaid expression of individual genes using a range of colors from yellow (not detected) to blue/purple (highest expression) using the FeaturePlot function as implemented in Seurat package in R. To determine the proportion of cells that express a given specifier gene, the which function in R was used to determine the number of cells within a cluster or group of clusters with expression values greater than 0. To determine the proportion of RPs that express a given number of specifier genes, a subset of the gene expression matrix containing the expression levels of 17 manually curated specifier genes in only the cells of the RP clusters was used. The number of expressed specifier genes in each RP was determined using the colSums function in R. Histograms were plotted using GraphPad Prism 6 software. To determine the average expression level of specifier genes *Brn1* and *Tle4* in RPs compared to neurons, a subset of the expression matrix containing only the RPs and neurons that expressed the aforementioned specifier genes was used and the average expression level for each gene was determined using the rowMeans function in R.

QUANTIFICATION AND STATISTICAL ANALYSIS

Microscopy and quantification

Analysis of cell culture and brain sections were performed as previously described (Wang et al., 2010). Briefly, cells grown on glass coverslips were analyzed with a Zeiss Axioplan2 microscope. For quantification, 100-300 EGFP-positive transfected cells per condition were counted and results from at least three independent experiments were analyzed. For the analysis of embryonic brains with in utero electroporation, at least 3 anatomically matched sections per brain from at least 3 embryos of 2 to 3 independent mothers for each condition were imaged with a 20X objective on an Olympus IX81 fluorescence microscope equipped with a Hamamatsu C9100-13 back-thinned EM-CCD camera and Okogawa CSU X1 spinning disk confocal scan head. Images were processed by using Volocity software (Perkin Elmer) and Adobe Photoshop CS6. Pax6, Tbr2 and Hoechst staining were used to define to the ventricular zone (VZ), subventricular zone (SVZ) and cortical plate (CP). Costes' test for colocalization was performed using ImageJ's "Just Another Colocalization Plugin" (JACoP) (Costes et al., 2004; Bolte and Cordelières, 2006). In brief, the test creates randomized images by scrambling pixels of the green channel. This process is repeated 200 times, and the Pearson correlation coefficient (r) is calculated every time between the scrambled image of the green channel and the original unscrambled red channel image. The measured correlation coefficient of the original unscrambled image is subsequently compared to the distribution of correlation

coefficients of the randomized images and a probability (P value) is calculated. p > 95%/0.95 suggests significant true colocalization (Costes et al., 2004).

Statistics

Sample sizes (n) indicated in figure legends 3A, 4B and supplemental figure legends 5A,B and 6A,B correspond to the number of independent experiments analyzed (n = 3). Sample sizes (n) indicated in figure legends 2D, 2E, 3H, 3I, 5, 6, 7, 8, S4, S6C, and S6D correspond to the number of embryos from at least two independent mothers analyzed (n = 3-4). All data were expressed as the mean plus or minus the standard error of the mean (SEM), unless otherwise indicated. With the exception of the microarray data, statistical analyses were performed with a two-tailed Student's t test or, where relevant, ANOVA with Dunnett's or Tukey's post hoc tests, using GraphPad Prism 6 software. For gene ontology analysis, p values were determined by DAVID. For the RIP-microarray analysis, the p values were adjusted with the Benjamini-Hochberg method in R. For the Pum1/2 motif analysis, p values were determined by the Wilcoxon rank sum test. p value < 0.05 was considered significant. In all figures, asterisks denote statistical significance *p < 0.05, **p < 0.01,***p < 0.001.

DATA AND SOFTWARE AVAILABILITY

The Pum2 RNA-immunoprecipitation expression data have been deposited in the GEO database under ID code GEO: GSE108404.